Journal of Building Engineering 98 (2024) 110781

Contents lists available at ScienceDirect

Journal of Building Engineering

journal homepage: www.elsevier.com/locate/jobe

Hybrid modular construction system "INNO3DJOINTS": Experimental behaviour and numerical modelling of isolated sub-frames

Nemanja Milovanović [a,*], Trayana Tankova [b], Rui Simões [a], Luís Carlos Silva [a], Hélder David Craveiro [a], Ricardo Costa [a], Cláudio Martins [a], Luís Simões da Silva [a]

[a] ISISE, Civil Engineering Department, University of Coimbra, Portugal
[b] Department of Engineering Structures, Delft University of Technology, Netherlands

ARTICLE INFO

Keywords:
Modular construction
Prefabrication
Plug-and-play steel joints
Hybrid steel structures
Full-scale tests
Numerical model

ABSTRACT

With the growing demand for sustainable, cost-effective and overall-efficient building solutions, the need for dependable modular construction systems is steadily on the rise. In the present paper a novel hybrid modular construction system named INNO3DJOINTS is introduced, employing cold-formed welded steel tubular columns, fabricated according to EN 10219, and cold-formed steel thin-wall section based truss-girders, joined by the innovative plug-and-play (P&P) connector, designed to provide ease-of-assembly and -disassembly. The experimental investigation conducted on isolated sub-frame configurations of the novel system is presented, where 6 full-scale specimens were subjected to horizontal and vertical loading. The test configurations differed in the P&P joint socket thickness and the absence/presence of the light steel framing (LSF) wall, encased with oriented strand board (OSB). In addition, a numerical model for predicting the system's global behaviour is proposed, developed in SAP2000. Initially, the behaviour of the employed P&P joint configurations, categorized as partial-strength, is characterized using experimental and validated ABAQUS finite element model (FEM) data, resulting in a spring model implemented into the global FEM. Finally, the numerical and experimental results are compared and discussed, leading to conclusions regarding the system's 2D structural performance, identified behaviour governing phenomena, P&P joint influence, LSF wall and OSB contribution, as well as the capabilities of the developed FEM.

* Corresponding author. ISISE, Department of Civil Engineering, University of Coimbra, Polo II, Rua Luís Reis Santos, 3030, Coimbra, Portugal.
E-mail address: milovanovic.nemanja@uc.pt (N. Milovanović).

https://doi.org/10.1016/j.jobe.2024.110781
Received 8 September 2023; Received in revised form 10 August 2024; Accepted 15 September 2024
Available online 19 September 2024

NOTATION

Latin symbols	
E	Young's Modulus of Elasticity
F	Force
f_u	Steel Ultimate Strength
f_y	Steel Yield Strength
G	Shear Modulus of Elasticity
$k_{1.axial}$, $k_{2.axial}$	Joint Axial Spring Stiffness
$k_{hor.EC.SLS}$	Estimated Eurocode Serviceability Limit State Horizontal Stiffness Demand
$k_{vert.EC.SLS}$	Estimated Eurocode Serviceability Limit State Vertical Stiffness Demand
$K_{e.hor}$	Initial Elastic Horizontal Stiffness
$K_{e.vert}$	Initial Elastic Vertical Stiffness
M	Bending Moment
Greek symbols	
δ	Displacement
υ	Poisson Ratio
Φ	Joint Rotation
Φp	Plug Rotation
Φs	Socket Rotation
Abbreviations	
(D)	Screw Diameter
SD	Self-Drilling Screw
BC-I/II/III	Boundary Conditions I/II/III
C	Lipped Channel Section
C-1, C-2	Column 1, Column 2
CFS	Cold-Formed Steel
CLT	Cross-Laminated Timber
DoF	Degrees of Freedom
E, F	Elastic (E), Failure (F)
EC3	Eurocode 3
EC3-1-3	Eurocode 3 Part 1–3 (EN1993 Part 1–3)
Eq.	Equation
EXP	Experimental
FC1, FC2, FC3	Frame Configuration 1/2/3
FC1-H-E	Sub-frame configuration FC1, loaded horizontally (H), in the elastic range (E)
FC1-V-F	Sub-frame configuration FC1, loaded vertically (V), until failure (F)
FE	Finite Element
FEM	Finite Element Model
FO	Frame Object
Fu.EC3	Ultimate Load according to Eurocode 3
GNA	Global Nonlinear Analysis
H, V	Horizontal, Vertical
HRS	Hot-Rolled Steel
HJ	Hydraulic Jack
LC	Load Cell
LO	Link object
LSF	Light Steel Framing
LVDT	Linear Variable Displacement Transducers
MC	Modular Construction
MoE	Modulus of Elasticity
NUM	Numerical
NZEB	Near-zero energy buildings
OSB	Oriented Strand Board
OSB/2	Oriented Strand Board Class 2
P&P	Plug-and-Play
PL	Preload
R3	Rotation in Z direction
RP1, RP2, RP3	Reference points 1, 2 and 3
Ref.	Reference
S8, S10	Socket with nominal thickness of 8 mm/10 mm
SG	Strain Gauges
SLS	Serviceability Limit State
SHS	Square Hollow Section
Tol	Tolerance
T-plug.tol	Initial clearance between the socket and the T-plug i.e. installation tolerance
T-plug.tol0	Initial clearance between the socket and the T-plug set to be 0 mm
T-plug.tol2	Initial clearance between the socket and the T-plug set to be 2 mm
U1	Translation in X direction
Z_{arm}	Lever arm

1. Introduction

Modular construction (MC) has been on the rise in the last decades, representing a fast, economic and sustainable construction concept. It refers to the industrialized production of pre-engineered 1D (element), 2D (panel) and 3D (module) building units, delivered on-site and assembled as large volumetric components or substantial elements [1–4]. The most commonly used MC systems rely on the exclusive or combined application of 2D panelised and 3D volumetric units, as they allow for the highest level of prefabrication (above 90 % [5]), with the latter at times delivered fully-complete. Characterised by elaborate planning, prefabrication, quality-controlled production and standardized installation routines, MC enforces increased building quality, speed and safety; ease-of-assembly and construction convenience; reduced site labour, construction time and terrain occupancy (up to 50–60 % [6]); and reduction in used energy, resources and produced waste (especially on-site, even up to 90 % [5,7,8]). Moreover, the detailed design nature of MC promotes the consideration of all life cycle stages, therefore envisioning recycling, reuse and/or facility repurposing, leading to cost-effective solutions with reduced environmental impacts [5,9–12].

Despite having a great potential, MC makes for a small portion of the construction market share, no more than 5–10 % in countries such as Germany, United States of America, United Kingdom and Australia [8]. Several challenges, with their impact intertwined, hinder the efficiency of MC, affecting its structural, constructional, economic, environmental, safety and regulatory aspects. The cost-effectiveness of MC is maximized in objects with large number of repetitive building units, characteristic for high-rise structures, however, modular solutions currently account for less than 1 % of them [13]. Indeed, the lack of an efficient lateral-load supporting system and high-performing joints, marked as the main structural issues of MC [14,15], together with the lack of detailed design/-construction guidelines, especially for multi-storey buildings [16], limit the use of fully modular structures to low-rise application, impeding its competitiveness.

Next to the need for joints with high strength and stiffness [5], studies on MC connections emphasize that a market-appealing joint solution needs to ensure economic detailing, streamlined manufacturing processes, standardization and convenient on-site assembly/disassembly [14,15]. Recent investigations converge towards the conclusion that bolted joints, with self-aligning and self-locking features, preferably detachable, represent the best suited connection typology to fulfil the MC demands. However, several significant challenges are identified, such as ensuring vertical and horizontal diaphragm continuity, insufficient joint ductility and failure to comply with seismic design requirements. Likewise, the necessity of controlling the installation tolerances is highlighted, suggesting limits of up to 2 mm for both horizontal and vertical connections, in order to prevent global failure due to slip accumulation over the structure's height [15,17–19].

The competitiveness of MC systems is also strongly influenced by the solution's size and weight, known indicators of environmental impact and cost, underlying the importance of optimal material, cross-section and member typology selection. Steel-timber hybrid prefabricated systems are proving highly promising in this regard, representing a lightweight, aesthetically pleasing, economically and energetically efficient solutions, based on recyclable/reusable materials [2,8,20–22].

The use of solid wood panels, such as cross laminated timber (CLT), as structural floors and walls is noted in numerous MC systems [23–26]. CLT panels offer sufficient structural stability and rigidity, while being at times over 50 % lighter than its concrete counterpart, with a superior capacity-to-weight ratio [27,28]. Moreover, their use results in low environmental impact, facilitated processing and assembly. In Refs. [29,30], CLT panel-steel beam floor system [30] and CLT panel-steel bracing lateral load resisting system [29] were applied to multi-storey case study buildings, showcasing hybrid steel-timber solutions as optimal in terms of both structural and environmental performance, with potential to fulfil the near-zero energy building (NZEB) demand. One steel-timber system is presented in Refs. [28,31], employing CLT panels, strengthen with cold-formed steel (CFS) profiles, as shear walls and floor diaphragms, enabling easy panel installation and replacement.

When it comes to steel, CFS has found a widespread use in MC. The flexibility, economy and capacity-to-weight efficiency it provides, leading to savings of up to 35 % over hot-rolled steel (HRS) [32], resulted in the emergence of lightweight steel frame (LSF) construction systems [33,34], relying strongly on panelised CFS elements. Joining CFS profiles into panels, such as LSF walls, floors and light truss-girders [35], results in increased in-plane stiffness, and therefore, larger free spans and improved lateral stability, while the utilization of sheathing (often wood-based) and/or cross-bracing can further enhance the performance under lateral loading [7,35–37]. Moreover, novel panels being investigated show promise in improving the inherent fire resistance limitations and overall performance of LSF systems for NZEB application, without compromising its structural behaviour [38,39]. However, even so, purely LSF based construction systems are rarely used outside of low-rise structures, as the problems of insufficient lateral stiffness and strength for mid- to high-rise application persist [40].

Likewise, a great number of MC systems rely on the use of hollow section members, most often as the chassis of corner supported modules [19]. Indeed, tubular sections are efficient in providing lateral stability, given their high stiffness and resistance in both planes, and allow height/span expansion without altering the outer member dimensions, by thickness variation, providing aesthetic advantages.

To capitalize on the benefits of hollow section members and address the limitations of LSF, hybrid solutions are being explored. The hybrid wall panel system studied in Refs. [7,41,42], combining HRS tubular section based rectangular panel, resisting lateral loads, and LSF panel, participating in sustaining the vertical loads, outperformed the traditional moment resisting frame and LSF solutions in the conducted multi-storey building case studies, leading to savings of nearly 40 % on the structural steel and being around 35 % cheaper. Moreover, one system employing tubular columns, extended via a patented sleeve connection, and CFS truss-girders, together with LSF walls for reinforcing the spans, was found commercially available [43], marketed as a solution suitable for mid-rise structures.

Despite the recent efforts and implied potential of a hybrid MC solution employing tubular sections, thin-wall CFS members, and

wood-based panels, not many construction systems rely on their combined use as primary structural elements. This is largely so given the connection execution and design difficulties, particularly of column-to-column [44] and beam-to-column joints. Indeed, the Eurocode's component method is not validated for characterization of bolted joints including CFS members [45,46].

The present paper introduces a novel hybrid modular construction system, employing tubular columns, CFS truss-girders, LSF walls, CLT slabs and an innovative bolted "plug-and-play" (P&P) beam-to-column connection. The system was developed under INNO3DJOINTS research project framework [47], aiming at addressing the discussed MC limitations and market necessitates.

The objective of the study reported herein was to characterize the 2D behaviour of the novel system, identify the key response governing parameters and develop a numerical model suitable for its representation. Firstly, an experimental investigation conducted on a representative full-scale substructure of the system (sub-frame), under horizontal and vertical loading, is presented. Both open and closed sub-frame solutions were tested, with 2 joint configurations employed, allowing to assess the joint, LSF wall and OSB sheathing contribution. Subsequently, FEM development was carried out, in 2 steps. In the 1st step, the (i) P&P joint characterization was performed, based on experimental data [48] and simulations run on a validated ABAQUS FEM, leading to a lumped spring model (0D). In the 2nd step, a global frame model was developed in SAP2000, with the joint spring model incorporated in it. Finally, the experimental and numerical results are elaborated, compared and discussed.

2. Description of the novel modular construction system

The conceptual idea behind the INNO3DJOINTS system was to develop a lightweight innovative modular construction system suitable for low and mid-rise structures, characterized by ease-of-transportation, -handling and –assembly, which can be reused, repurposed and/or recycled. To do so, several member typologies and materials are employed, matched to achieve high efficiency in their role, resulting in a hybrid system.

As the elements of the structural frame, the INNO3DJOINTS system employs (i) tubular columns and (ii) thin-walled CFS truss-girders (Fig. 1), exploiting the best features of both components, i.e. the high stiffness/resistance in both planes and the efficiency in the load-carrying capacity, respectively. The beam-to-column connection is established by the newly developed (iii) P&P joint (Fig. 2), providing secure and easy installation. Additionally, the system envisions the use of cross-laminated timber (CLT) slabs (iv), due to their favourable in-plane stiffness and capacity-to-weight ratio, as well as the (v) LSF walls, encased with oriented strand boards (OSB), as part of the lateral load resisting system.

The P&P connector has the role of providing ease-of-assembly and immediate functionality. It is composed out of 3 main parts; (i) socket, (ii) plug and a (iii) pair of bolts. The socket comes welded to the column, while the plug leaves the workshop bolted to the truss-girder. The connection is established on site, by sliding the plug into the socket and fastening them together with a pair of bolts.

3. Experimental campaign

3.1. Overview

A two-part experimental campaign was conducted on the INNO3DJOINTS system, consisting of (i) full-scale sub-frame tests and (ii)

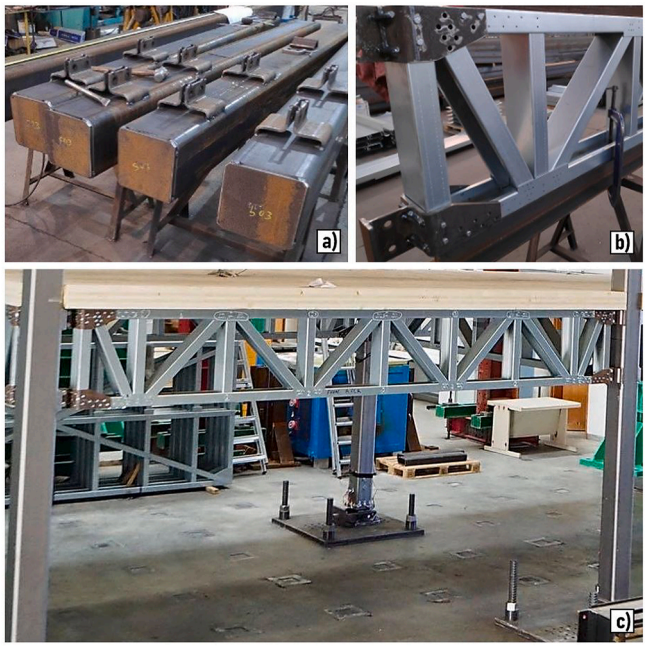

Fig. 1. The INNO3DJOINTS system: a) columns with the socket welded; b) truss-beam with the plug attached and c) the system post-assembly.

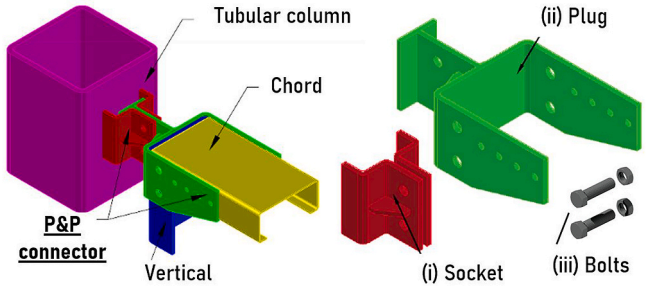

Fig. 2. Visual illustration of the P&P joint and its components.

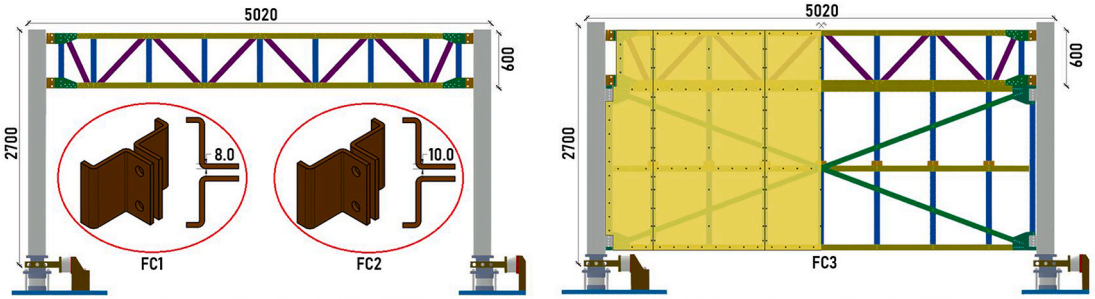

a) Open-frame configurations (FC1 and FC2) b) Closed-frame configuration (FC3)

Fig. 3. Isolated sub-frame specimen configurations (dimensions in mm).

full-scale building tests, with the former pertaining to the scope of the present paper.

A total of 6 sub-frame specimens (3 unique configurations with 2 specimens of each) were tested under (i) horizontal (H) and (ii) vertical (V) loading. The configurations (Fig. 3) differed in the P&P joint socket thickness and the LSF wall absence/presence. Reflecting the prevalent solutions used in the real-world application, two frame typologies, open and closed, were chosen for experimental examination. Configurations 1 (FC1) and 2 (FC2) employed P&P-S8 and P&P-S10, respectively, and represented the open hybrid frame solution, used to gauge the system's potential to provide, next to the structural functionality, unobstructed useable space and architectural flexibility. Configuration 3 (FC3) was formed by adding a LSF wall, encased with OSB boards, to the FC2, and represented the closed hybrid frame solution, used to assess mainly the system's potential to provide stiffness under horizontal actions, contributing to the definition of its scope of use. The specimens underwent 2 test repetitions, the initial one in elastic range (E), and the final one, until reaching the ultimate capacity (F). The employed nomenclature is given in Table 1.

3.2. Specification of the experimental specimens

3.2.1. Materials and fabrication

The structural materials employed for forming the specimens included (i) HRS, (ii) CFS and (iii) OSB. Hot-rolled S355NH steel plates served as the base material for producing the tubular columns, conforming to EN 10219, and P&P joint components, using cold-forming and welding in the process. Thin-walled profiles, used for forming the truss-girders and the LSF walls, were made of cold-formed S350GD + Z class steel. OSB class 2 (OSB/2) was employed for encasing the LSF walls.

3.2.2. Plug-and-play joint configurations

At the initial stage of the project, pre-designed P&P joint configurations were tested and analysed using FEM, at the component level. Based on the obtained results, the P&P joint specimen geometry was determined, followed by an experimental campaign reported in Ref. [48].

Two of the tested P&P joint configurations, namely E-S8-W1 (here designated as P&P-S8) and E-S10-W1 (here designated as P&P-

Table 1
Specimen and test nomenclature.

Specimen	Frame Config.	*P&P Config.*	*Load*	Test 1	Test 2
FC1-H	FC1	P&P-S8	Horizontal (H)	Elastic (E)	Failure (F)
FC2-H	FC2	P&P-S10	Horizontal (H)	Elastic (E)	Failure (F)
FC3-H	FC3	P&P-S10	Horizontal (H)	Elastic (E)	Failure (F)
FC1-V	FC1	P&P-S8	Vertical (V)	Elastic (E)	Failure (F)
FC2-V	FC2	P&P-S10	Vertical (V)	Elastic (E)	Failure (F)
FC3-V	FC3	P&P-S10	Vertical (V)	Elastic (E)	Failure (F)

Note: To exemplify the used designation, FC1-H-E refers to the sub-frame configuration FC1, loaded horizontally (H), in the elastic range (E).

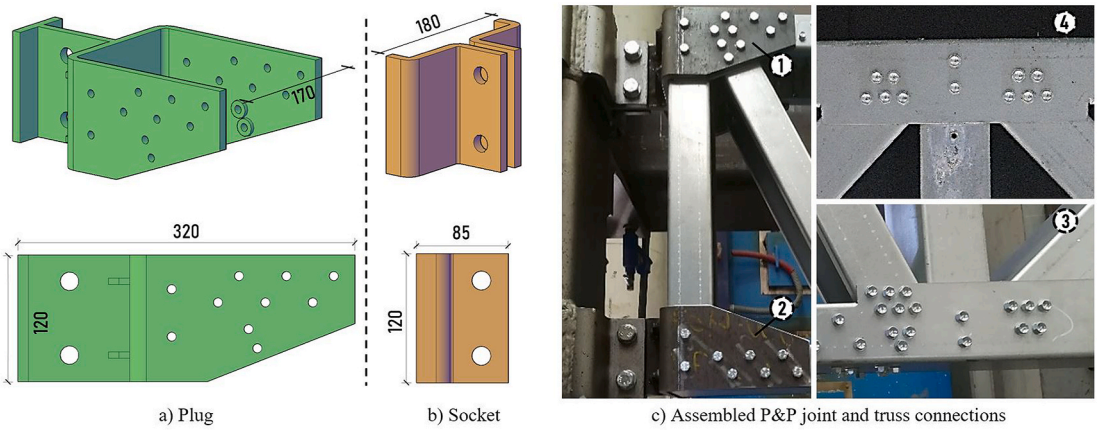

Fig. 4. Assembled P&P joint and truss connectivity. Socket and plug dimensions.

S10), belonging to the equal-strength group, were selected for use in the sub-frame specimens, as solutions which facilitate production and contribute to cost reduction by not having stiffeners, while fulfilling the estimated target resistance load for residential and office buildings in non-seismic areas. The two configurations differed only in the thickness of the socket, which equalled 8 mm in the case of P&P-S8 and 10 mm for P&P-S10. Both configurations employed 2 M16 class 8.8 bolts and had the remaining dimensions, of both the socket and the plug, identical (Fig. 4). The plug-to-truss connection was established via M8 class 8.8 bolts.

3.2.3. Specimen geometry and member typologies

Prior to defining the final specimen configurations, case studies were conducted on the sub-frame (2D) and building (3D) finite element model (FEM), with the aim of optimizing the INNO3DJOINTS solution. The case studies [49] focused on evaluating the optimal floor system, horizontal and vertical load-bearing systems, truss-girder and column typologies, cross-section shape and size, as well as the effects of span length, number of spans and presence of LSF walls with OSB.

The reached conclusions lead to adopting cold-formed square hollow sections (SHS) for columns, with cross-section dimensions of 200x200×10 mm, and "Warren" type truss-girder, composed of 2.5 mm thick lipped channel (C) thin-walled profiles, as the member typologies forming the sub-frame specimens. Lipped channel C150x65x20x2.5 mm profiles were employed as the truss chords, while C145x65x20x2.5 mm profile was used for the truss verticals and diagonals. The chords were internally reinforced near their edges with a CFS 2.5 mm thick U profile, spreading between the first 2 verticals. The columns had a height of 2700 mm, while the truss-girder spanned 4365 mm. The distance between the external edges of the upper and the lower chord of the truss-girder equalled 600 mm, as well as the distance between the centroids of the verticals. The connection between the CFS truss members was established by 6.3(D) self-drilling (SD) screws. All vertical-to-chord connections employed 2 screws, while the diagonal-to-chord connection had 2 variations (Figs. 4 and 5). The truss design resulted in eccentric element intersection at the truss nodes. The eccentricities ranged from 8 to 72

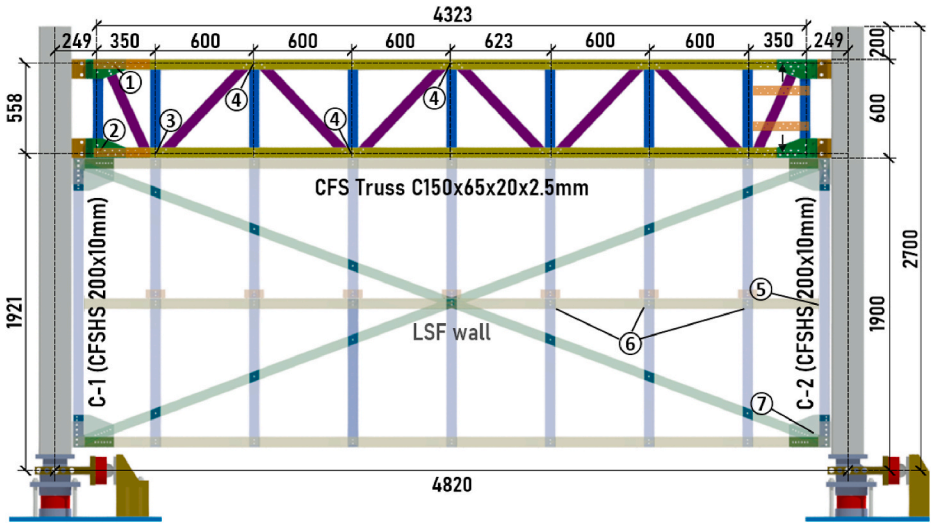

Fig. 5. Sub-frame specimen geometry with respect to member centroids. Connection numbering.

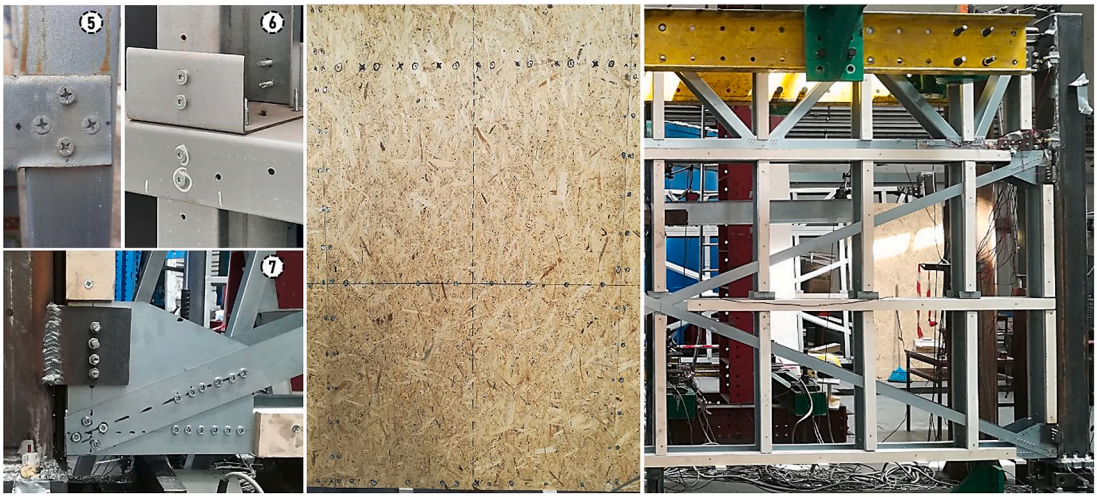

Fig. 6. The LSF wall. The employed connections, OSB panel with screws positioning and pre-OSB installation layout with wood spacers.

mm, relative to the element centroids.

The same thin-walled profiles were used to build the LSF wall panels, together with 60×2.5 mm CFS cross-bracing straps and 12.5 mm thick OSB boards. The walls were made as an isolated system component, out of 9 vertical studs, positioned exactly below the verticals of the truss-girder (600 mm spacing), and 3 horizontal joists, resulting in a panel spanning 4620 mm with 1760 mm of height (Fig. 7), without considering the installation tolerances. Cross-bracing straps were added on both sides of the wall for increasing the horizontal stiffness. The wall elements were joined by screws, with CFS 2.5 mm thick gusset plates facilitating the connections in the corners (Fig. 6).

The employed member cross-sections and materials used in the experimental campaign are summarized in Table 2.

3.2.4. *Light-steel framing wall assembly*

The connection between the sub-frame and the LSF wall was established, on one side, via bolted plate connection, joining the frame columns and the LSF wall edge studs, and, on the other, by screwing the top wall joists to the bottom chord of the truss (Figs. 6 and 7). Two pairs of 10 mm thick HRS S355 plates were welded to the SHS columns at the wall corner level, making sockets, and the column-to-wall connection established by 4 M8 bolts (class 8.8). After installing the bare LSF wall, the OSB was added as the wall envelope,

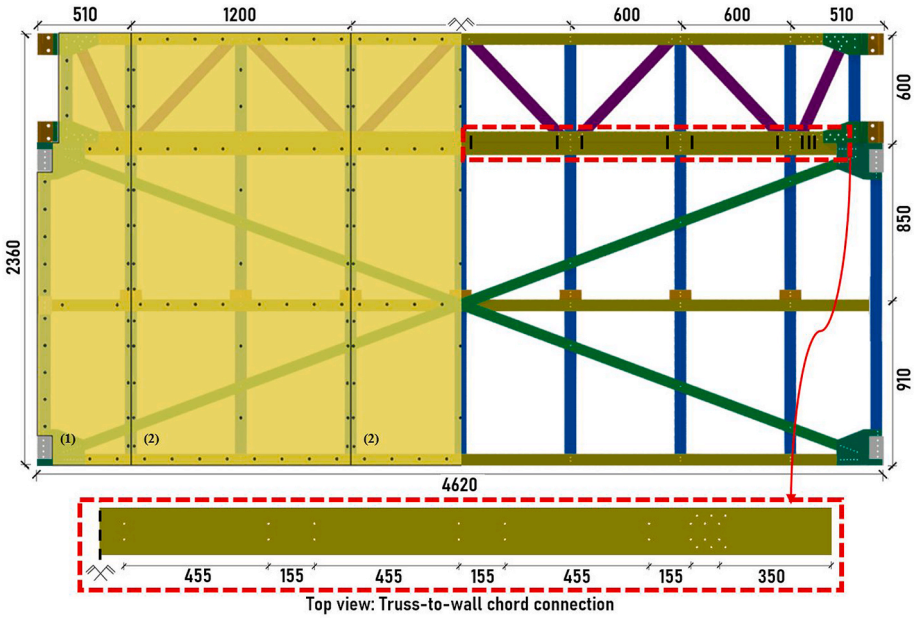

Fig. 7. The LSF wall with OSB, assembled below the truss-girder (nominal dimensions).

Table 2
Profiles and materials used in the experimental campaign.

Structural Element	Cross-Section	Dimensions	Material
Columns	Square Hollow Sections	200x200x10 mm	HRS S355NH
Truss-Girder (Chords)	Lipped Channel "C"	150x65x20x2.5 mm	CFS S350GD + Z
Truss-Girder (Ver/Diag)	Lipped Channel "C"	145x65x20x2.5 mm	CFS S350GD + Z
LSF wall (Joists)	Lipped Channel "C"	150x65x20x2.5 mm	CFS S350GD + Z
LSF wall (Studs)	Lipped Channel "C"	145x65x20x2.5 mm	CFS S350GD + Z
Cross-bracing (LSF_{wall})	Rectangular	2 x 60x2.5 mm	CFS S350GD + Z
P&P Joint	Rectangular	120x8/120x10 mm	HRS S355NH
OSB	Rectangular	12.5 mm	OSB/2

Note: All CFS-CFS and CFS-OSB connections were established by 6.3(D) SD screws.

Table 3
LSF wall geometry and screw spacing.

Dimensions (span x height)	*Installation* Tolerances	*Screw No.* (OSB-to-CFS)	*Screw spacing* (Edge, OSB-to-CFS)	*Screw spacing* (Other, OSB-to-CFS)
4610x1750 mm	10 mm	2x 270	150 mm	150–400 mm

covering both the wall panel and the truss-girder.

For one side of the frame, 5 panels were used, 2 panels of configuration (1) and 3 of configuration (2), as given in Fig. 7, made out of 4 OSB boards with dimensions of 2400x1250x12.5 mm. In order to overcome the wall-to-OSB offset, created by the P&P plug, gusset plates and fasteners protruding from the rest of the frame, 18 mm thick wood spacers were attached to the LSF wall prior to assembling the OSB. The screw spacing of the OSB-to-CFS connection varied depending on the location. At the sub-frame edges, spacing of 150 mm was used, at the edges of the OSB panels the employed spacing was 150–200 mm, while the screw distance in the interior varied from 150 to 400 mm.

Figs. 6 and 7 illustrate the LSF wall configuration, post-assembly layout and the OSB board shapes, dimensions and screw positioning. The nominal LSF wall dimensions were reduced in the production process due to the consideration of installation tolerances (Table 3).

3.3. Experimental layout

The horizontal load test set-up (Fig. 8) consisted of the specimen itself, reaction wall, hydraulic jack, 2 auxiliary frames and lateral restrain for the top chord of the truss. The experimental sub-frames were installed next to the reaction wall, to which a hydraulic jack (HJ) with a load cell was attached, positioned at the column top, aligned with the truss-girder top chord. Two auxiliary frames were employed to attach a beam (UPN 300) providing the out-of-plane restraint for the upper chord of the truss-girder, simulating the effect of a slab. The column bases were connected to the rigid ground plates, fixed to the reaction slab, through a reaction measuring system, positioned in between. The end support conditions allowed for free in-plane rotation.

The vertical load test layout was organized in a similar way (Fig. 9). The column-to-ground plate connection remained the same,

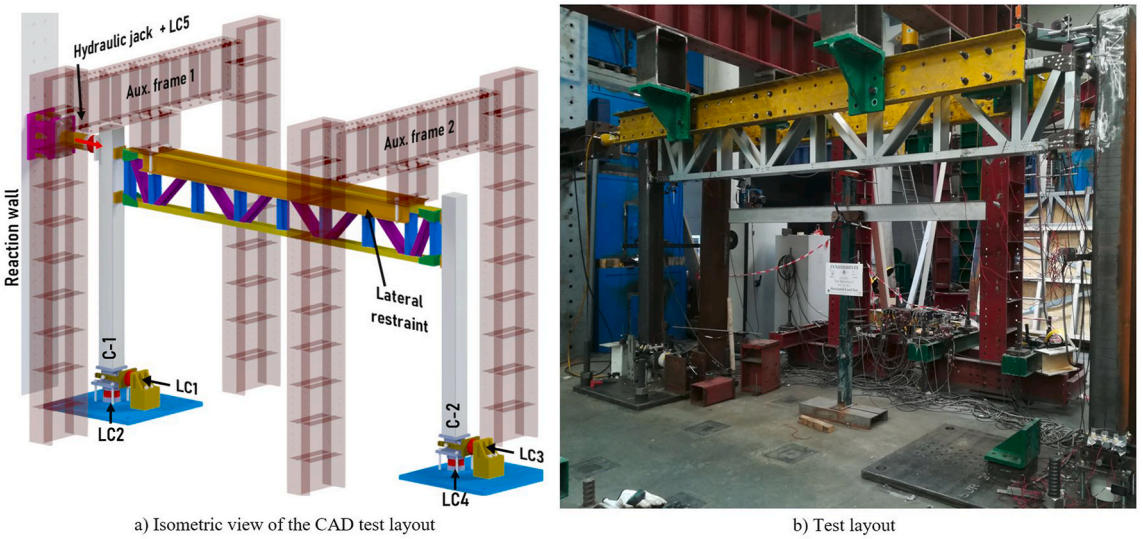

a) Isometric view of the CAD test layout b) Test layout

Fig. 8. Experimental layout of the isolated sub-frames subjected to horizontal load.

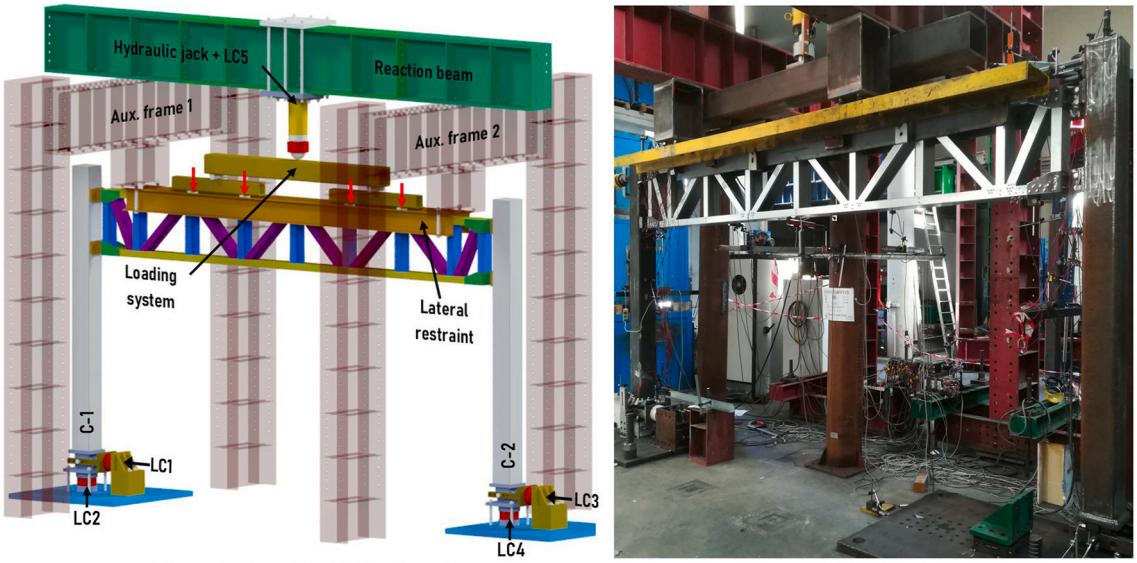

a) Isometric view of the CAD test layout b) Test layout

Fig. 9. Experimental layout of the isolated sub-frames subjected to vertical load.

providing pinned support conditions. The upper truss chord out-of-plane restraint was maintained. Unlike in the horizontal load test layout, an additional element was employed, the reaction beam, used for attaching the hydraulic jack above the specimen. The load was transferred from the HJ, through the load cell measuring the applied load, to the load-transferring system made of rigid beams, performing a 6-point bending test. Each beam had 2 cylinders welded on it, transferring the load to the specimens, at 4 points. The cylinders were centred with respect to the axes of the truss-girder verticals, in order to minimize eccentricities.

3.3.1. *Relevant layout details*

The contact between the specimen and the out-of-plane displacement restraining beams was established through a set of rollers (Fig. 10a), attached to the restraining beams, in order to minimize the friction.

The experimental layout included a reaction (vertical and horizontal) measuring system, installed at the level of column supports (Fig. 10b). The support plates contained a slotted hole, allowing the horizontal slip and thus load transfer to the LCs.

Throughout the experimental campaign, alterations to the layout were made affecting the boundary conditions (BCs). In the initial test layout, the horizontal translation at column supports was limited only by the extent of the slotted hole. For specimens FC2-V and FC3-V, the outward horizontal translation of column C-1 was restrained (BC-I), by a vertical plate, welding to the ground plate. Likewise, steel plates were added below the load-transferring pins (BC-II) in order to avoid excessive deformation due to load concentration. For testing FC3-V, vertical supports were provided below the LSF wall studs (BC-III).

Fig. 10 depicts the discussed layout details, while a summary of the test specimens and corresponding BC alterations is given in Table 4.

3.4. *Instrumentation*

As measuring instruments, linear variable displacement tranducers (LVDTs), strain gauges (SGs) and load cells (LCs) were employed. The LVDTs were used to measure the absolute displacements of the truss-girder (in-plane and out-of-plane), columns

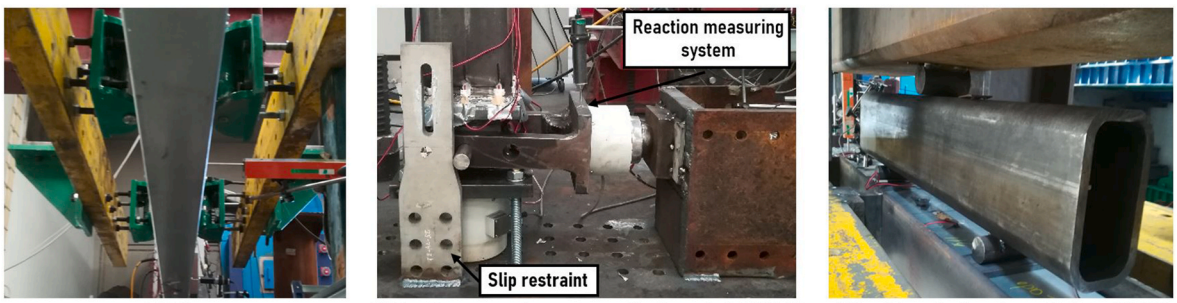

a) Rollers b) Reaction measuring system with slip restraint (BC-I) c) Load transferring pins and plates (BC-II)

Fig. 10. Relevant layout details.

Table 4
Experimental campaign summary, particularities and target loads.

Specimen	LSF [Y/N]	OSB [Y/N]	*Added BCs (I), (II), (III)*	Test 1	Test 2
FC1-H	No	–	–	12.5 kN (E)	(F)
FC2-H	No	–	–	12.5 kN (E)	(F)
FC3-H	Yes	Yes	–	20.0 kN (E)	(F)
FC1-V	No	–	–	40.0 kN (E)	(F)
FC2-V	No	–	*(I), (II)*	40.0 kN (E)	(F)
FC3-V	Yes	No	*(I), (II), (III)*	40.0 kN (E)	(F)

Note: Specimen FC3-H underwent an additional test repetition in the elastic range, denominated FC3-H-0, prior to installing the OSB, which is not included in Table 4. The aim was to assess the OSB contribution to the horizontal stiffness.

(horizontal and uplift) and support plates, while also measuring the relative displacement of the truss edge with respect to the columns, representing the P&P joint deformation. The SGs were used for strain measurements in the truss elements, P&P joint sockets, at column bases and in cross-diagonal bracing strips (in the case of FC3 specimens), while having the reactions and the applied force measured by the LCs, positioned near the column supports and attached to the HJs, respectively.

Fig. 11 depicts the position of the instrumentation considered relevant for understanding the specimen behaviour. For the purpose of demonstrating the horizontal displacement at the load application level, relevant for calculating stiffness, the fictive LVDTs 5.1* and 5.2* are introduced. Their data was obtained by processing the nearby LVDT 5.1 and 5.2 readings.

3.5. Test procedure

The load was applied through the hydraulic jack, using displacement control, simulating quasi-static loading conditions, in both vertical and horizontal load tests. In general, 2 test repetitions were conducted on each specimen, aiming at ensuring the test layout and result validity. The 1st test repetition was in the elastic range, in which the specimens underwent a loading/unloading cycle, using a loading rate of 0.001 mm/s. The elastic range test was used for verifying the experimental layout and instrumentation, eliminating gaps and recording the preliminary elastic response of the frames. In the 2nd repetition, the load-bearing capacity was assessed, with the loading rate increased to 0.01 mm/s.

Table 4 summarizes the experimental campaign, giving the specimen and layout particularities, as well as the respective target loads of elastic tests, obtained from preliminary FE analysis.

3.6. Experimental results and discussion

3.6.1. Horizontally loaded frames

The experimental behaviour of the specimens loaded horizontally is described by presenting the recorded horizontal displacement (LVDTs 3–5*, Fig. 12), strain (Fig. 13) in the vicinity of the failure governing elements throughout the loading stage and the post-failure deformed configurations (Figs. 14–16). For the sake of horizontal stiffness evaluation, comparison with numerical results and transparency, both raw measurements and processed data (excluding slip) are presented. The initial elastic horizontal stiffness ($K_{e.hor}$) was evaluated for each sub-frame column (C1/C2), using LVDT 5* measurements (load application level). Certain LVDTs were exhausted during testing, hence the lack of data up to the ultimate load.

The behaviour of specimens FC1-H and FC2-H was characterized by linear-elastic response up to roughly 23 kN of load applied (Fig. 12), after which non-linearity is noted, governed by the P&P joint. The estimated initial elastic horizontal stiffness ($K_{e.hor}$), given in Table 5, was 0.94/0.94 kN/mm and 1.13/1.17 kN/mm for FC1-H and FC2-H, respectively, indicating a contribution of P&P-S10 to the overall frame stiffness of 20–25 %, when compared to P&P-S8. As a result of significant internal deformation within the joint, most notably socket bending, the T-plug came into contact with the column (Fig. 14) at approximately 50–55 kN of load applied, leading to an additional change of slope, in both specimens. The socket width closely matched the width of the column, resulting in negligible contribution of column face out-of-plane deformation to the overall deformation of the joint.

Finally, the load-bearing capacity of FC1-H and FC2-H was reached for 78.9 kN and 76.7 kN of load applied, respectively. The failure of FC1-H was observed in the node of the compressed segment of the truss, in the bottom chord, with the combined local buckling and net-section tearing as the governing phenomena (Fig. 14). Accordingly, a rapid rise of strain, measured in the vicinity by SG16-17-18 (Fig. 13), can be noted from 60 kN of applied load. Similarly, the failure of FC2-H occurred due to the local buckling of the compressed truss elements, this time on both sides of the specimen. On one side, of the lower chord, in the same node as in FC1-H, with the net-section tearing less pronounced, and on the other, of the top chord, again in the truss node (Fig. 15). Accordingly, the SGs recorded somewhat different stress/strain distribution. It was concluded that the failure of both specimens occurred due to the stress concentration near the truss nodes, exacerbated by the presence of eccentricities.

No significant plastic deformation of the columns was noted, nor of the CFS elements prior to the failure. Likewise, no significant out-of-plane displacement was recorded in either of the specimens, with the maximum value being 4 mm in the case of FC2-H, at ultimate load.

The behaviour of the frame FC3-H (Fig. 12), equipped with LSF wall and OSB, was characterized by a less pronounced elastic stage, largely due to many sources of slip, as a consequence of high number of fasteners/gaps. The $K_{e.hor}$ (Table 5) was estimated as 13.3/20.3 kN/mm. Additionally, in order to estimate the contribution of the bare LSF wall to the $K_{e.hor}$, test FC3-H-0 was conducted prior to installing the OSB, resulting in $K_{e.hor}$ of 6.33/7.1 kN/mm (FC3-H-0 results are not presented in detail). By comparing the $K_{e.hor}$ of FC3-H with FC2-H, it can be concluded that the presence of the bare LSF wall, without OSB, increases the $K_{e.hor}$ of the frame by 5.5–6 times.

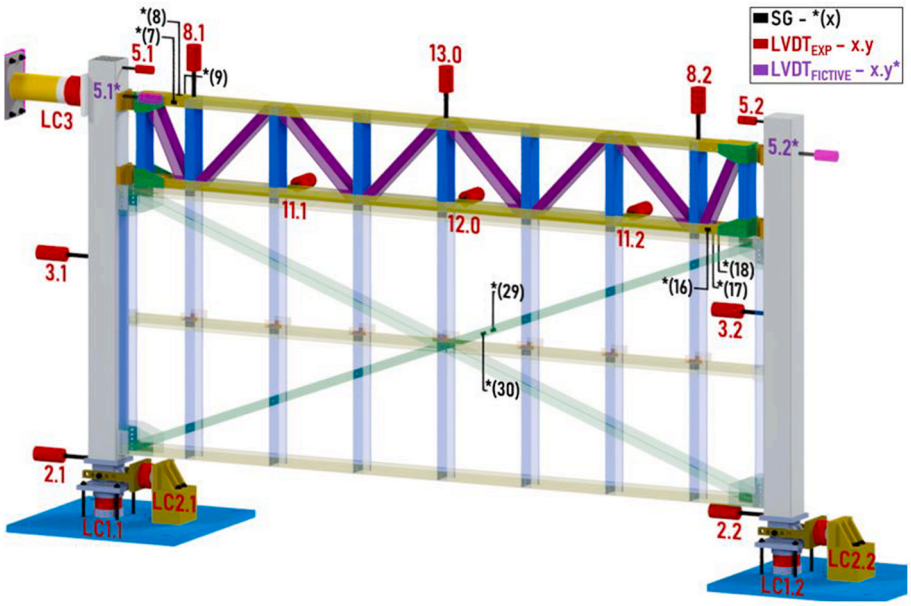

a) Sub-frame instrumentation for horizontally loaded specimens FC1-H, FC2-H and FC3-H

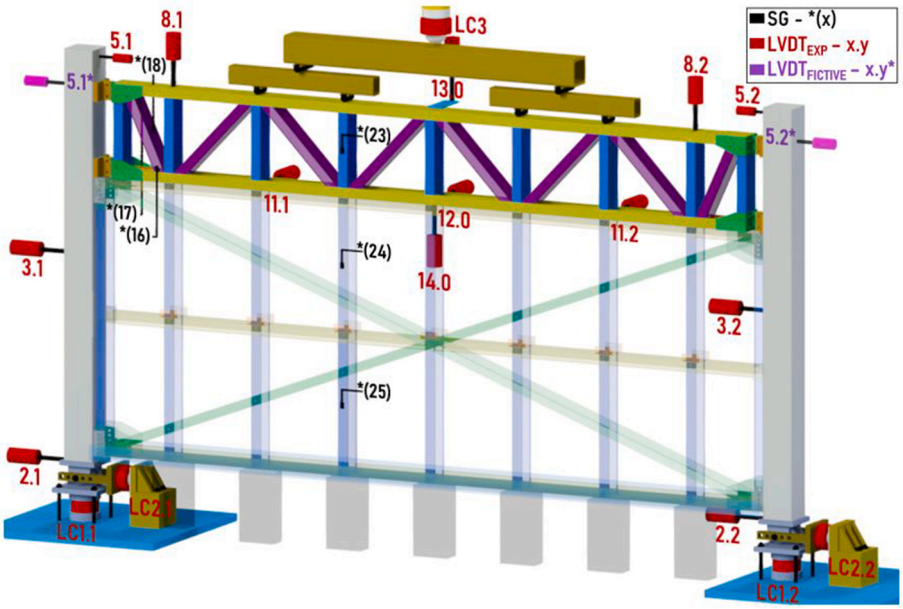

b) Sub-frame instrumentation for vertically loaded specimens FC1-V, FC2-V and FC3-V

Fig. 11. Relevant instrumentation used in sub-frame tests.

Moreover, significant contribution of the OSB was recorded, as encasing the bare LSF wall with 2×12.5 mm thick OSB panels more than doubled the $K_{e.\ hor}$ obtained in FC3-H-0, resulting in the $K_{e.hor}$ increase of 11.5–17 times when compared to a wall-less frame.

The load-bearing capacity of FC3-H was reached for a load of 269.9 kN and corresponding horizontal displacement of 70 mm, as measured by LVDT 5.1*, which represents an increase in capacity of approximately 3.5 times, when compared to FC2-H. The failure of FC3-H was progressive, as the robust nature of the specimen allowed for alternative stress/force pathways after a localized failure. It was possible to confirm that the collapse initiated in the column-to-wall connection (Fig. 16). The bolts in shear started successively failing at approximately 200 kN of load applied, causing fluctuations in the measured load (removed from the figures, but partially visible in Fig. 13d), while the entire connection suffered failure when approximately 220 kN of applied load was reached. After the test, the OSB panel was removed and additional phenomena observed, such as the LSF wall edge stud distortional deformation in the vicinity of the failed connection (Fig. 16b), local buckling of the compressed truss top chord, located above a vertical (Fig. 16c) and

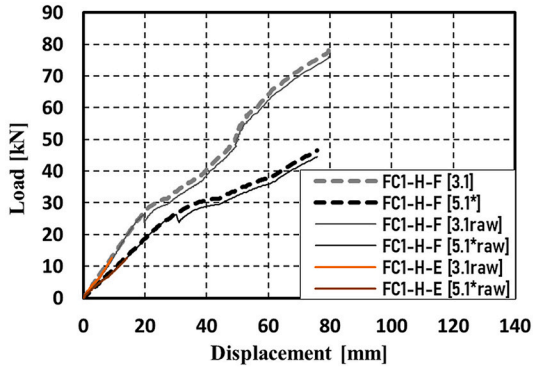

a) FC1-H (LVDTs 3.1-5.1*)

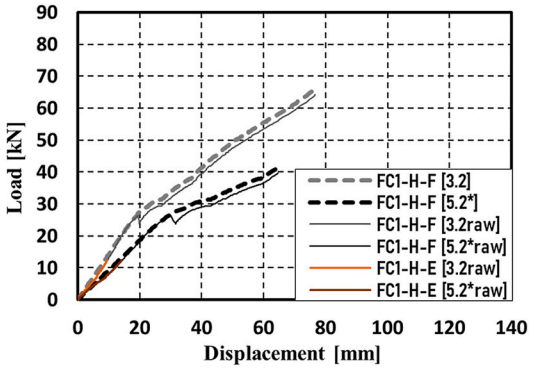

b) FC1-H (LVDTs 3.2-5.2*)

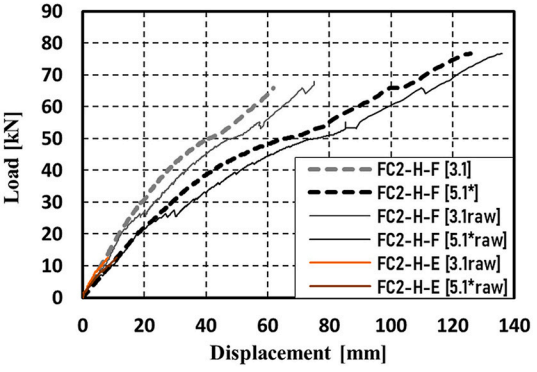

c) FC2-H (LVDTs 3.1-5.1*)

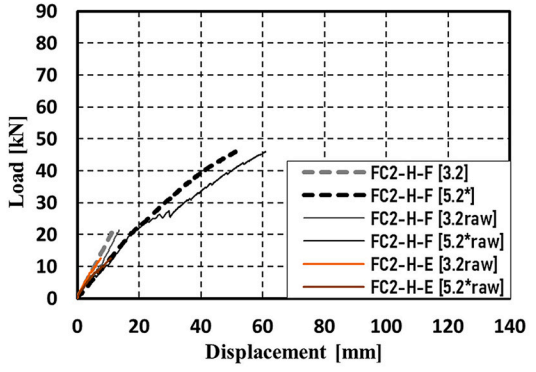

d) FC2-H (LVDTs 3.2-5.2*)

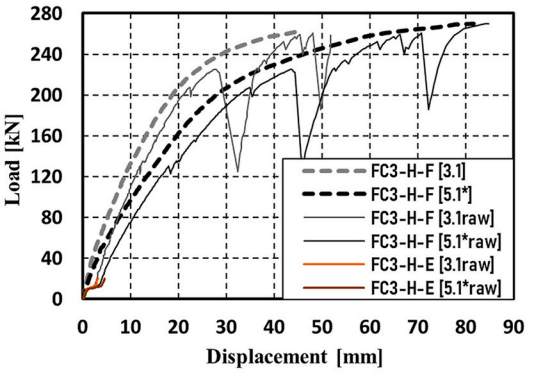

e) FC3-H (LVDTs 3.1-5.1*)

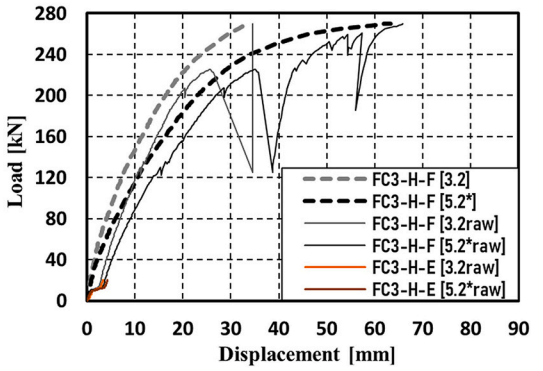

f) FC3-H (LVDTs 3.2-5.2*)

Fig. 12. Horizontal displacement of FC1-H, FC2-H and FC3-H (LVDTs 3–5).

buckling of the LSF wall bottom chord in compression (Fig. 16d). The SGs 7-8-9 measurements indicate (Fig. 13) that the latter phenomena governed the ultimate capacity of the specimen. The OSB remained intact until reaching near ultimate capacity, when a portion of it, in the lower-right corner, separated from the LSF wall, due to screw pull-through. Throughout the load application, gradual inter-panel shearing drift was noted. Maximum out-of-plane displacement recorded was 6 mm at ultimate capacity load.

3.6.2. Vertically loaded frames

The experimental response of vertically loaded specimens is presented by the measured horizontal displacement (LVDTs 2-3-5*, Fig. 17), vertical deflection (LVDTs 8-13-14, Figs. 17 and 18), strain (Fig. 19) in the vicinity of the failure governing elements and the post-failure deformed configurations (Figs. 20–22).

Specimens FC1-V and FC2-V varied only in employed P&P joint configuration, however, the test layouts differed in BCs, as summarized in Table 4 and described in **sub-chapter 3.3.1**. For both FC1-V and FC2-V, matching of the corresponding vertical

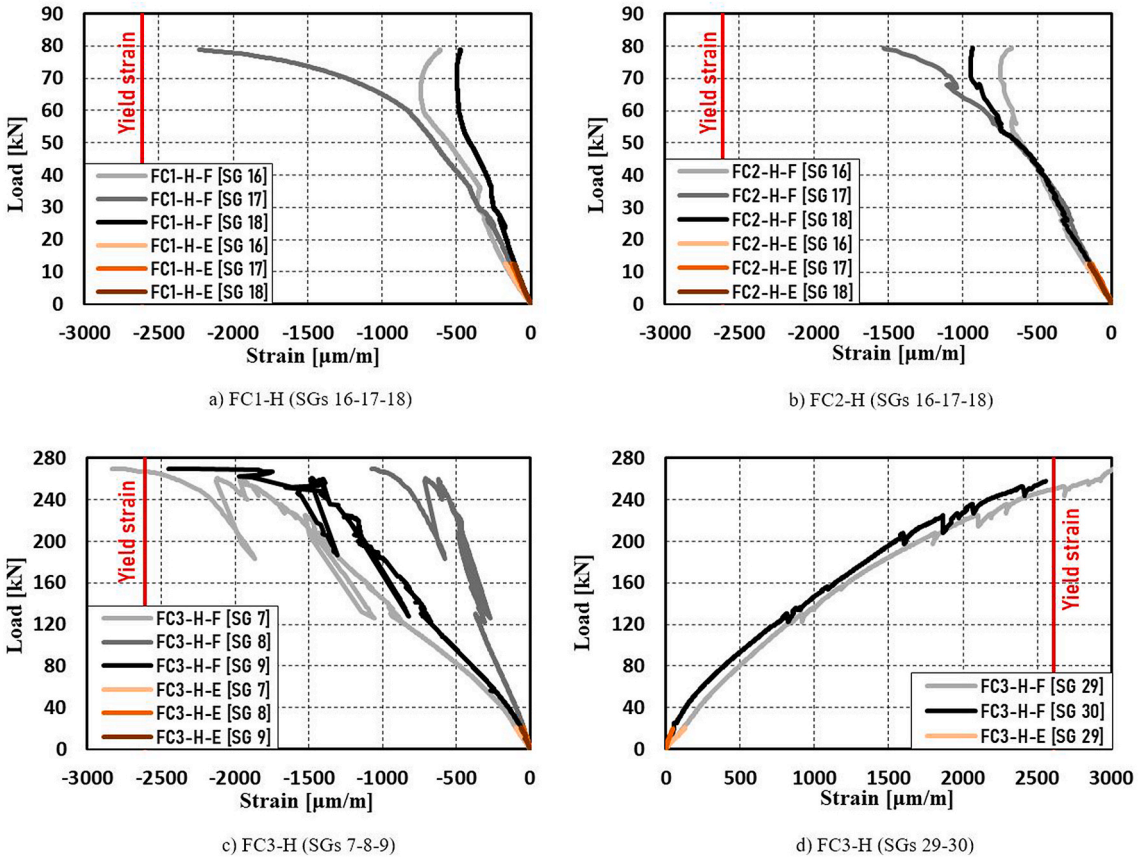

Fig. 13. Strain in the vicinity of the failure governing elements of FC1-H, FC2-H and FC3-H.

deflection measurements, namely LVDTs 8.1–8.2 and LVDTs 13.0–14.0, was recorded (Fig. 18), validating the expected symmetric behaviour of the specimen. No significant internal truss deformation was measured. Linear response was recorded up to around 50 kN of load applied, with the initial elastic vertical stiffness ($K_{e.vert}$) estimated at 10.1 kN/mm and 11.3 kN/mm (Table 6), for FC1-V and FC2-V, respectively, considering the total load applied and the LVDT 13.0 deflection.

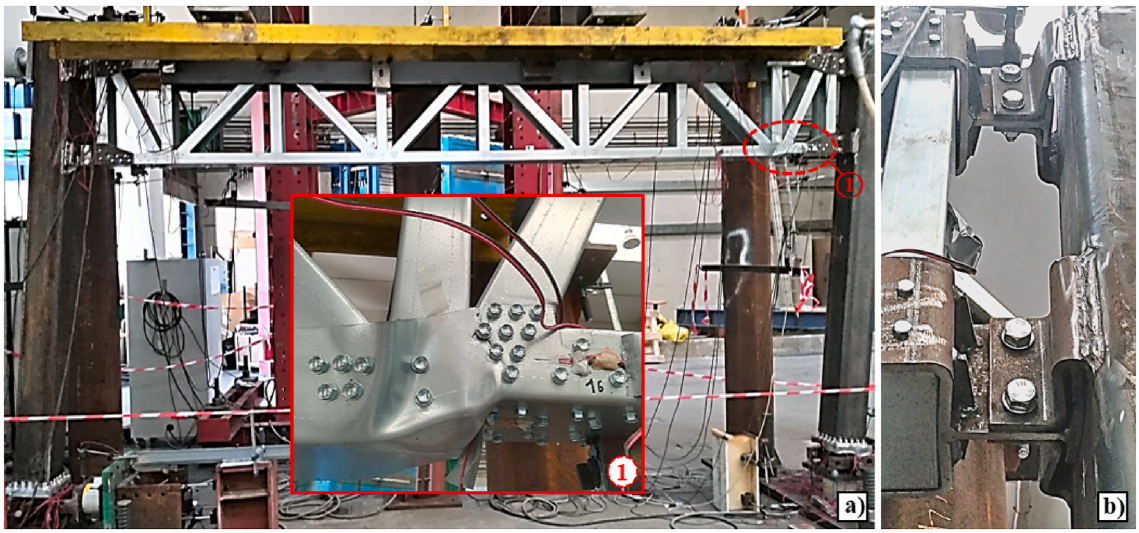

Fig. 14. Failure mode and post-test deformed configuration - FC1-H.

Fig. 15. Failure mode and post-test deformed configuration - FC2-H.

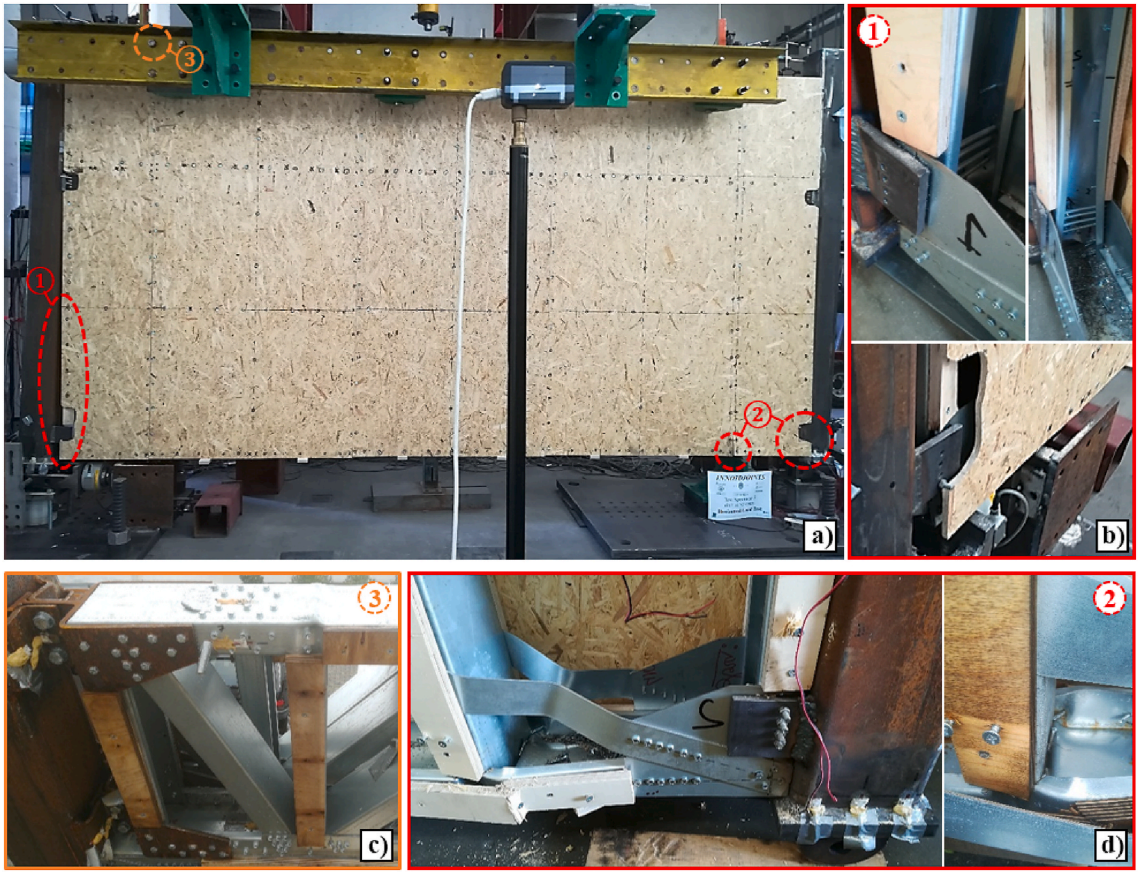

Fig. 16. Failure mode and post-test deformed configuration - FC3-H.

Table 5
Initial elastic horizontal stiffness (LVDTs 5.1*/5.2*) and ultimate capacity.

Test	FC1-H-F	FC2-H-F	FC3-H-0	FC3-H-F
$K_{e,hor}$ *[kN/mm]*	0.94/0.94	1.13/1.17	6.33/7.1	13.3/20.3
Ultimate capacity [kN]	78.9	76.7	–	269.9

Note: FC3-H-0 refers to an elastic range test conducted on FC3-H without OSB.

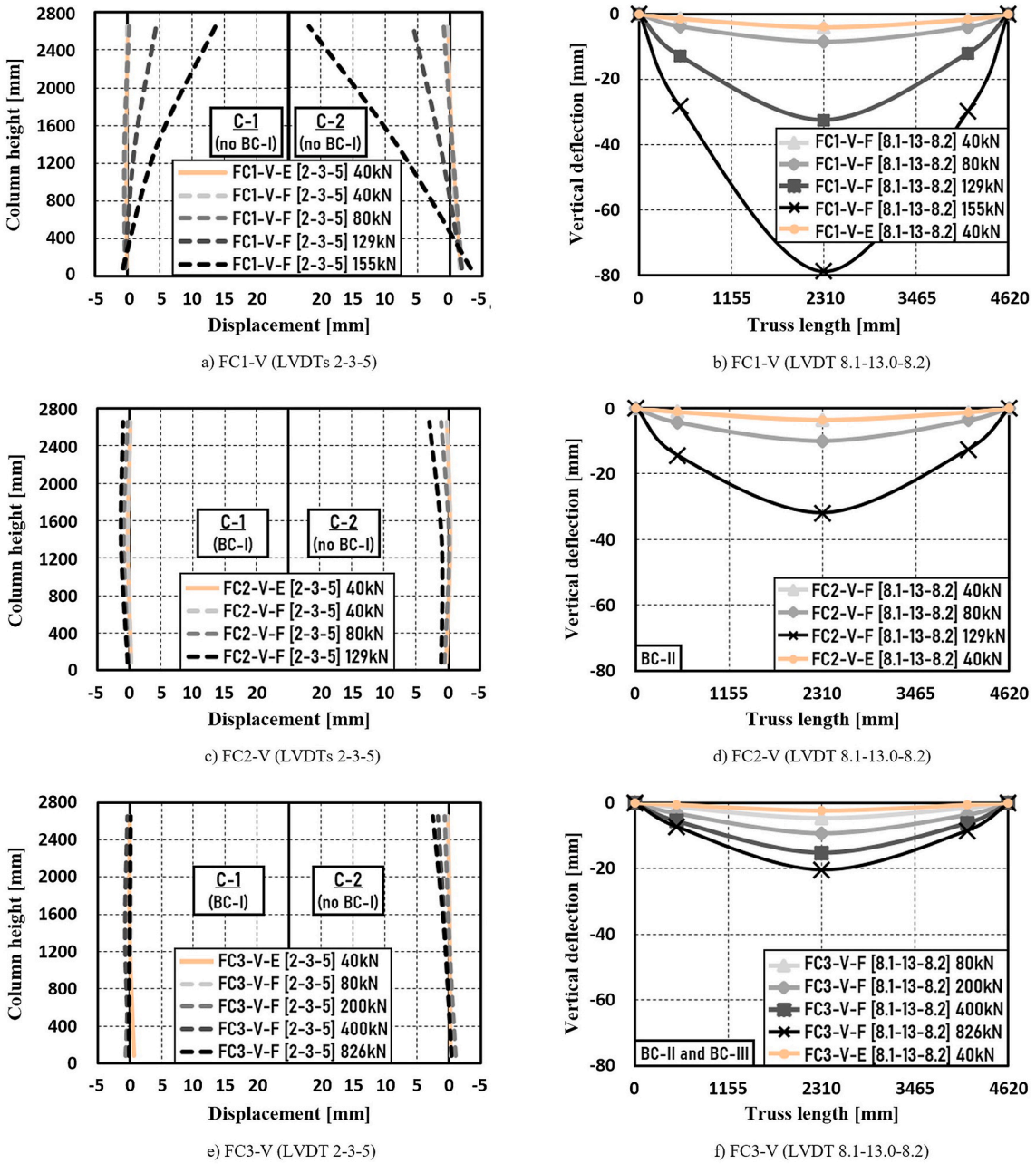

a) FC1-V (LVDTs 2-3-5)
b) FC1-V (LVDT 8.1-13.0-8.2)
c) FC2-V (LVDTs 2-3-5)
d) FC2-V (LVDT 8.1-13.0-8.2)
e) FC3-V (LVDT 2-3-5)
f) FC3-V (LVDT 8.1-13.0-8.2)

Fig. 17. Displacement and deflection throughout the column (LVDTs 2-3-5) and the truss (LVDTs 8.1-8.2-13.0) length - FC1-V, FC2-V and FC3-V.

At the 155 kN of applied vertical load, the load-bearing capacity of FC1-V was reached. Combined local buckling and net-section tearing of the truss lower chord (Fig. 20), in the node, was primarily responsible for the failure, similarly to the specimens loaded horizontally. No SGs were used in the proximity of the failed chord part, however, SG 16-17-18 (Fig. 19) were positioned symmetrically on the opposite side of the truss, giving therefore an indication of the strain development. In addition, as the load was

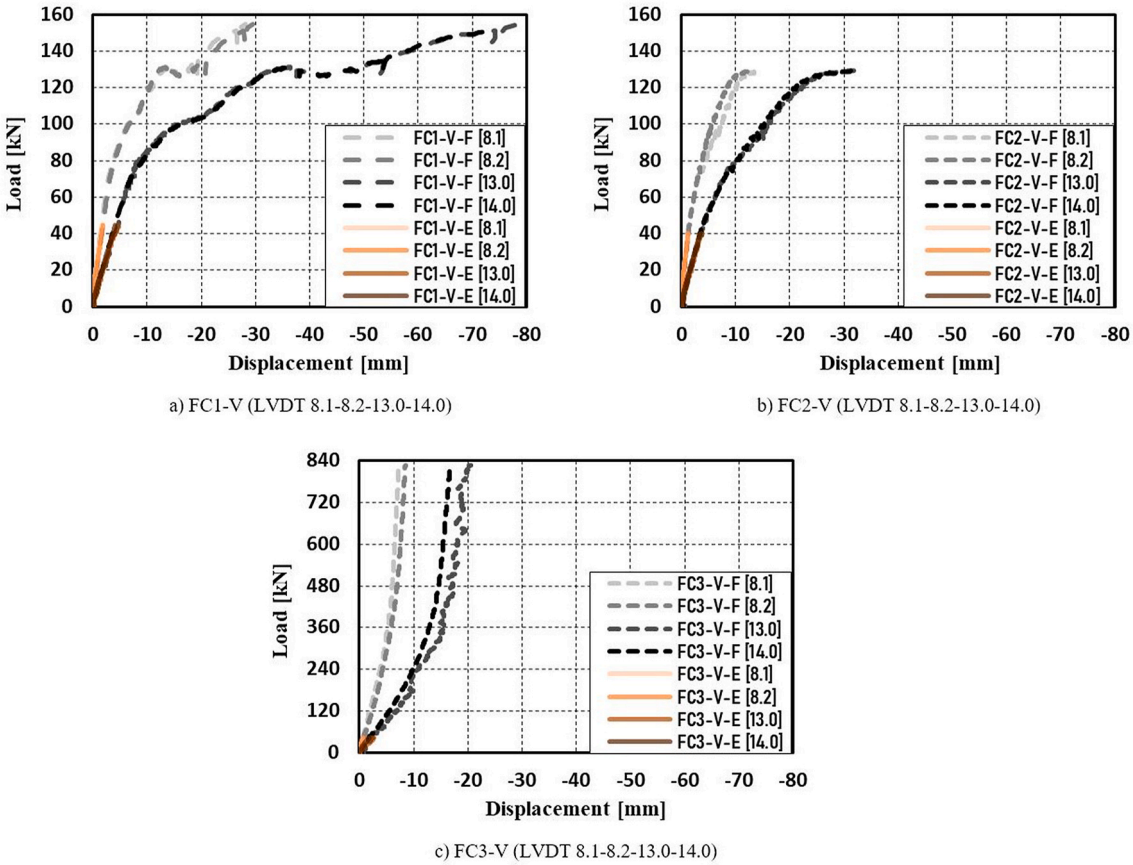

a) FC1-V (LVDT 8.1-8.2-13.0-14.0)

b) FC2-V (LVDT 8.1-8.2-13.0-14.0)

c) FC3-V (LVDT 8.1-8.2-13.0-14.0)

Fig. 18. Vertical displacement of FC1-V, FC2-V and FC3-V (LVDTs 8.1-8.2-13.0-14.0).

transferred directly from the pins to the top chord, excessive deformation was noted at the points of load application, as well as shearing of the whole truss segment between the load application points. The ultimate deflection at mid span, measured by LVDT 13.0, amounted to 78.4 mm. The load-bearing capacity of FC2-V was reached for 129 kN of applied vertical load, around 20 % lower than that of FC1-V, while again the combined local buckling and net-section tearing of the truss lower chord (Fig. 21), in the node, governed the failure. The SGs were again located on the opposite side compared to the capacity governing elements. Unlike in FC1-V, the excessive deformation at load application points and the shearing of the loaded segment were not noted in FC2-V, likely due to the application of the load-transferring plates (BC-II). The measured ultimate deflection at mid span was 31.9 mm, around 2.5 times lower than the one recorded in FC1-V.

The observed differences in the results between FC1-V and FC2-V in $K_{e.vert}$ (12 %), load-bearing capacity (20 %), deformed shape and deflection in the post-elastic stage, are believed to come from the mentioned BC variation. The lack of the slip restraint (BC-I) and the load-transferring plates (BC-II) in FC1-V, significantly affected the specimen's deformability and the deformed shape, resulting in a stress distribution which delayed the failure, allowing higher load to be sustained, in spite of the localized top chord deformation and "weaker" P&P-S8 joint utilization. The effect of the horizontal slip restraint can best be seen in Fig. 17, where the column deformed shape is given for various levels of applied load. In FC1-V-F, for higher load levels, an outward slip of the supports occurs, resulting in higher inclination of the columns and a different deformed shape when compared to FC2-V-F.

Given the layout differences, it is difficult to quantify the P&P joint socket thickness impact on the sub-frame vertical deformability; nonetheless, it appears that it had been minor. Contrarily, the presence of truss node eccentricities proved to have a governing effect on the discussed behaviour defining parameters. No significant plastic deformation of the column nor out-of-plane displacement was recorded in neither of the specimens.

The load-deflection (Fig. 18) response of the specimen FC3-V was characterized by the vertical stiffness increase with the increase of the applied load. The observed behaviour in the initial test stage was most likely a result of a cumulative slip, coming from large amount of fasteners, and thus gaps, which progressively got exhausted. In was not possible to eliminate the slip from the measurements.

The $K_{e.vert}$ (Table 6) was estimated as 16.52 kN/mm, obtained by considering the LVDT 13.0 measurements and the total load applied. The LSF wall presence had a strong influence on the ultimate capacity in FC3-V-F, as the failure occurred for 826 kN of load applied. The failure was governed by the buckling of the truss vertical (Fig. 22), positioned directly below load application point, to

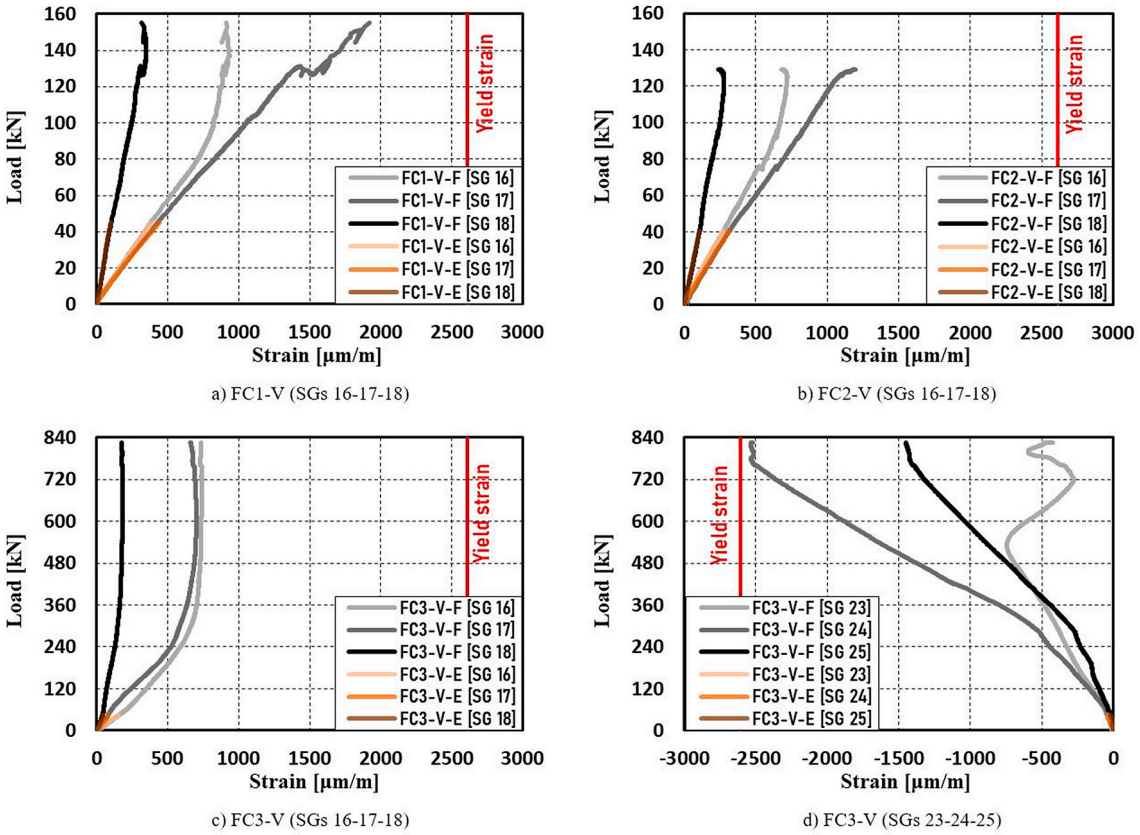

Fig. 19. Strain in the vicinity of the failure governing elements of FC1-V, FC2-V and FC3-V.

which SG 23 was attached. Moreover, due to high magnitude of the load applied, the top chord suffered excessive deformation at load application points, even with the load-transferring plates employed. The ultimate deflection at mid span, measured by LVDT 13.0, amounted to 20.4 mm, however, it should be noted that vertical supports were added below every LSF wall stud (BC-III). The horizontal slip restraint (BC-I) was present while testing FC3-V as well, resulting in a deformed shape of column C-1 similar to FC2-V, while C-2 exhibited slight outward slipping, as presented in Fig. 17. No significant plastic deformation was noted in the columns throughout the tests, while the maximum recorded out-of-plane displacement measured 14 mm, occurring for maximum load applied. The OSB was not installed on the FC3-V.

4. Numerical modelling

4.1. Model description, geometry and materials

With the purpose of developing a FEM capable of predicting the global behaviour of the INNO3DJOINTS sub-frame specimens, namely the initial stiffness, deformed shape and load-bearing capacity (by combining the obtained internal force distribution and EC3 steel member design provisions), commercially available software SAP2000 (v24) was used (Fig. 23).

The SHS columns, CFS truss-girder and LSF wall frame were represented by beam elements (1D FEs), referred in SAP2000 as frame objects (FO), defined by their cross-section and respective member centroid position, as given in Fig. 5. Accordingly, the truss element eccentricities were considered. Following the SAP2000 manual [50] suggestions, the approach "1 frame object = 1 structural element" was adopted, with automatic internal meshing. The OSB sheathing panels, assigned on both sides of the frame (Fig. 24), were modelled by area objects (2D orthotropic shell FEs), with a mesh of approximately 50x50 mm. In order to facilitate the meshing process and the connection to the frame, each OSB panel was represented by several area objects, joined together by applying area edge constrains.

Given the employed modelling strategy, the material properties of CFS and HRS were defined as isotropic elastic perfectly plastic, using the engineering stress-strain curve, obtained from the coupon tests. The contribution of the regions affected by cold-forming process was neglected. It is important to note that FOs do not support directly the consideration of material non-linearity, therefore global FE analysis did not include it. Yield (f_y) and ultimate strength (f_u) were only employed for performing design verifications. The OSB was modelled as elastic orthotropic material, with properties defined according to Ref. [51]. Mean values were adopted for modulus of elasticity (MoE) and shear modulus. Table 7 summarizes the assigned material properties.

The cross-sections assigned in FEM were based on nominal dimensions of the sections employed in the experimental campaign. The exception was the cross-bracing, where a single 60×4.92 mm rectangular section was used, instead of a double 60×2.5 mm section.

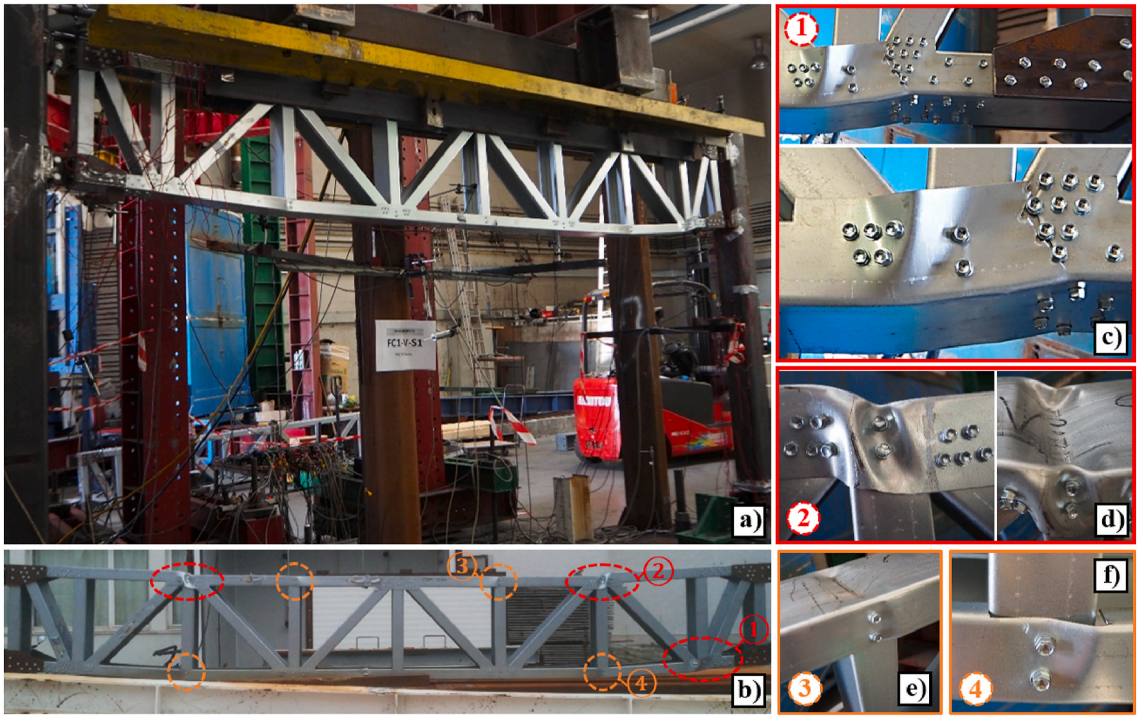

Fig. 20. Failure mode and post-test deformed configuration - FC1-V.

The reinforced parts of the truss were modelled as fully composite sections (Fig. 23). Table 8 gives a summary of the assigned sections and corresponding material properties.

4.2. Connections

The inter-element connectivity modelling can greatly influence the accuracy of FEM predictions [37,52–54]. For developing the INNO3DJOINTS sub-frame FEM, several connection modelling strategies were employed, with varying complexity levels, as summarized in Table 9. Special attention was given to the (i) beam-to-column P&P joint modelling, detailed in **sub-chapter 4.3.**

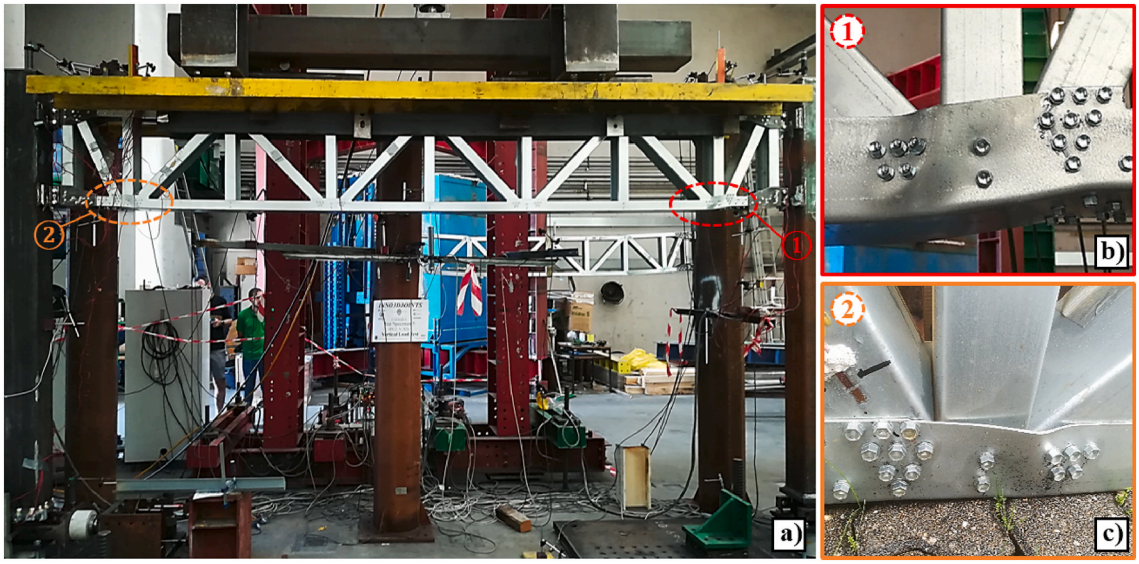

Fig. 21. Failure mode and post-test deformed configuration - FC2-V.

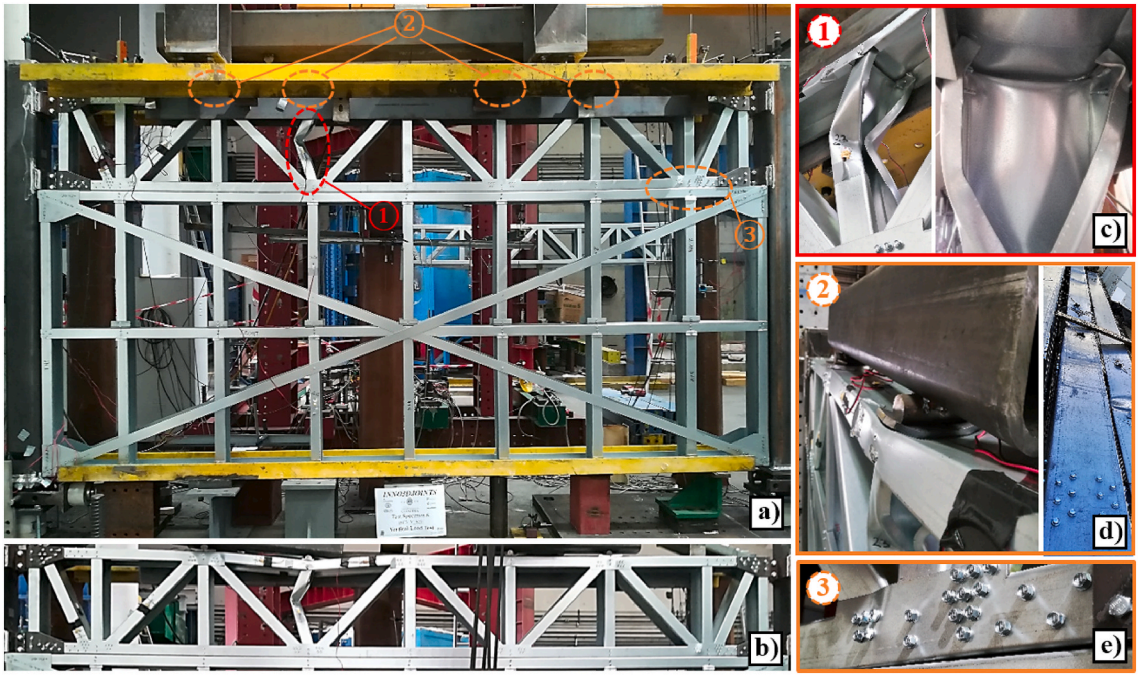

Fig. 22. Failure mode and post-test deformed configuration - FC3-V.

Table 6
Initial elastic vertical stiffness (LVDT 13.0) and ultimate capacity.

Test	FC1-V-F	FC2-V-F	FC3-V-F
$K_{e,vert}$ *[kN/mm]*	10.1	11.3	16.52
Ultimate capacity [kN]	155	129	826

The connection (ii) between the truss-girder elements (truss-to-truss), as well as the (iii) elements forming the LSF wall frame (wall-to-wall), was established by node formation at the element intersection and by assigning, when suitable, end moment releases. End moment releases were assigned to all the truss verticals and the LSF wall inner studs, as their connections employed only 2 fasteners, as well as to the wall middle joist and the cross-bracing (Fig. 23). The cross-bracing was, in addition, modelled to transfer only the axial tensions forces, by setting the compression limit to 0 kN. The remaining truss and LSF wall frame elements were connected assuming full continuity.

The connection between (iv) the truss lower chord and the LSF wall top track (truss-to-wall) was established below every truss vertical, by 4 screws, and near chord edges, on both sides, by 10 screws (Fig. 7). Though the 2 back-to-back C profiles seemingly form a built-up I section member, the literature [55] suggests that full composite action should not be expected for the screw spacing of 455 mm. Moreover, modelling the truss chord and the wall track as 1 beam FE would impose a change of strategy for the P&P joint modelling when LSF wall is used, due to the centroid offset. Therefore, in FEM, the truss chord and the wall track were modelled as individual members, connected by discrete FO based connectors (Fig. 24), restraining all relative deformation. The influence of the connection behaviour was taken into account through initial elastic shear stiffness, which was assigned to the rigid connector via end partial fixity springs (0D elements). The screw connection initial shear stiffness was estimated by applying the formula proposed in Ref. [56], considering the thread effect on the bolted shear connection stiffness. The approach was firstly validated against experimentally obtained stiffness of a single-lap screwed thin-plate connection in shear, given in Ref. [55], proving applicable, as the estimation resulted in a difference below 10 %. Each connector replicated the behaviour of a 4-screw or a 10-screw connection, with the estimated shear stiffness of 30 kN/mm and 76 kN/mm, respectively. The shear behaviour was implemented in FEM by assigning the shear partial fixity springs on both connector ends, which lead to attributing a doubled value of stiffness to each spring, as the 2 springs are in series.

The (v) column-to-wall connection i.e. the continuity between the column centroid and LSF wall stud was represented by a rigid FO, accounting for the connection eccentricity with respect to the LSF wall corner nodes. The estimated connection deformability was not introduced for the sake of simplicity, as considering it proved negligible.

The (vi) OSB-to-CFS connection was modelled by applying the concept presented in Ref. [53], where the connector behaviour is

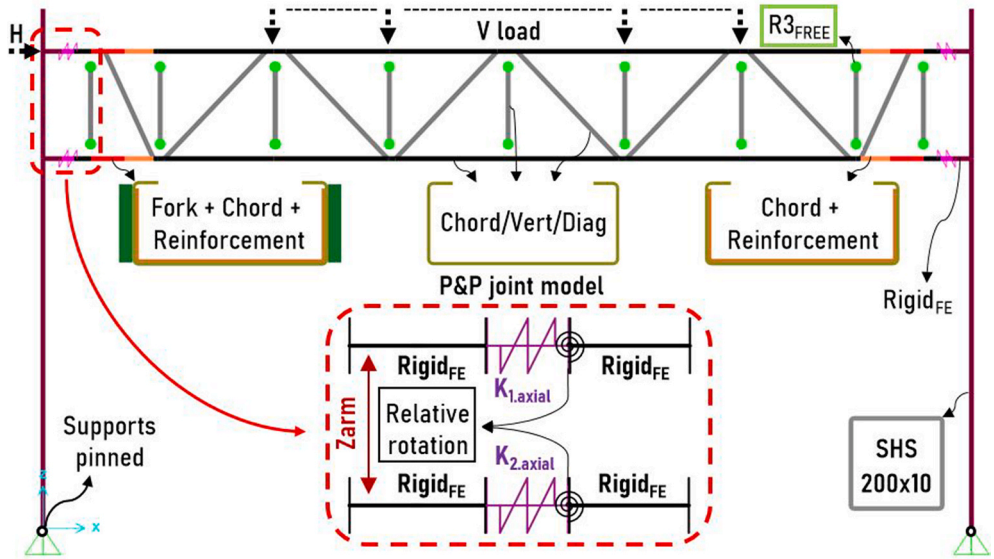

a) Open sub-frame solution FEM and the P&P joint.

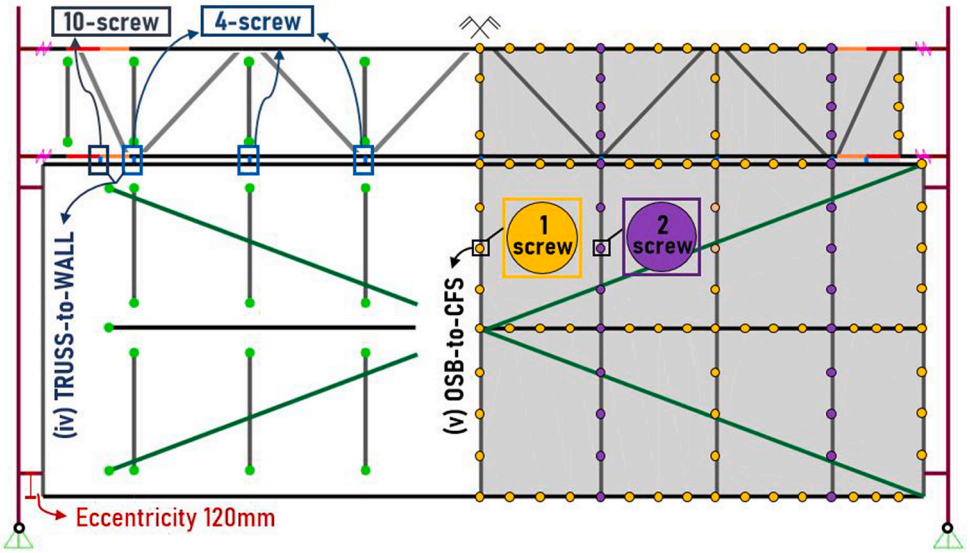

b) Closed sub-frame solution FEM. LSF wall modelling details.

Fig. 23. Global FEM and the P&P joint representation in SAP2000.

based on a single screw response. The connector was again represented by a rigid FO, of arbitrary length and with its centroid directed out-of-plane, while accounting for the connection behaviour by assigning shear partial fixity springs on both connector ends. As suitable behaviour of a single connector in shear, a stiffness of 0.9 kN/mm was adopted, a value in line with the experimental data found in the literature [37,53]. To clarify the FEM implementation, 1.8 kN/mm of shear spring stiffness was assigned at both connector ends, resulting in equivalent stiffness of 0.9 kN/mm. Partial fixity springs were considered in both shear directions. Some of the connectors located at the panel edge represented 2 screws, and thus used doubled value of stiffness. The connectors were distributed in a way to closely represent the experimental screw distribution (Figs. 23 and 24), with 52 connectors representing 2-screw connections and 146 connectors representing 1-screw connections on each side of the sub-frame model.

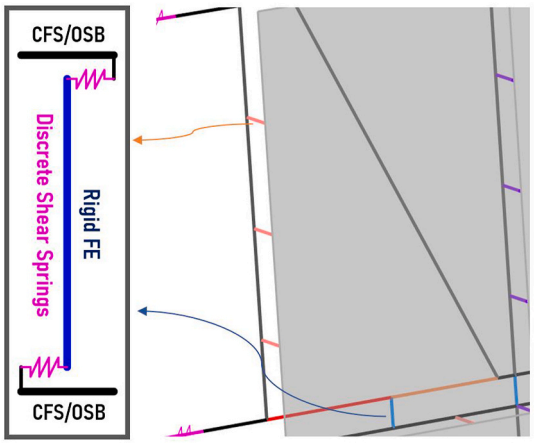

Fig. 24. Connector details and application - (iv) CFS-to CFS and (vi) OSB-to-CFS.

Table 7
Material properties assigned in FEM.

Material	*E [GPa]*	*G [GPa]*	υ	f_y	f_u	*Behaviour*
			[/]	*[MPa]*	*[MPa]*	*Model*
HRS S355NH	210	80.77	0.3	442	584	Elastic-Plastic
CFS S350GD + Z	203	76.32	0.3	530	610	Elastic-Plastic
OSB/2	$E_1 = 3.8$	$G_{12} = 1.08$	$\upsilon_{12} = 0.25$	/	/	Elastic-Orthotropic
	$E_2 = 3$	$G_{13} = 0.05$	$\upsilon_{13} = 0.25$			
	$E_3 = 3$	$G_{23} = 0.05$	$\upsilon_{23} = 0.3$			

Note: For OSB, elasticity modulus E_1 refers to the direction parallel to the wood fibre grain, E_2 to the direction perpendicular to the grain and E_3 to the out-of-plane direction. The same applies to shear modulus (G) and Poisson's ratio (υ).

Table 8
Profiles and material behaviour assigned in FEM.

Structural	*Finite*	*Assigned*	*Assigned*
Element	Element	Section	Material
Columns	1D (Frame)	(SHS) 200x200x10 mm	HRS S355NH (Elastic-Plastic)
Chords (truss)	1D (Frame)	(C) 150x65x20x2.5 mm	CFS S350GD (Elastic-Plastic)
Vert./Diag. (truss)	1D (Frame)	(C) 145x65x20x2.5 mm	CFS S350GD (Elastic-Plastic)
Tracks (wall)	1D (Frame)	(C) 150x65x20x2.5 mm	CFS S350GD (Elastic-Plastic)
Studs (wall)	1D (Frame)	(C) 145x65x20x2.5 mm	CFS S350GD (Elastic-Plastic)
Cross-bracing (wall)	1D (Frame)	(Plate) 60x4.92 mm	CFS S350GD (Elastic-Plastic)
OSB	2D (Shell)	2x (Plate) t = 12.5 mm	OSB/2 (Elastic Orthotropic)

Table 9
Summary of connection modelling in the FEM.

No.	Connection	Modelling Approach	Assigned Behaviour	Reference
(i)	*P&P joint*	Link Objects	Experimental Behaviour	[48]
(ii)	*Truss-to-Truss*	Centroid intersection	Continuity or End M releases	–
(iii)	*Wall-to-Wall*	Centroid intersection	Continuity or End M releases	–
(iv)	*Truss-to-Wall*	Rigid FO Connector with shear springs	Initial shear stiffness (30 or 76 kN/mm)	[56]
(v)	*Column-to-Wall*	Rigid FO	Continuity	–
(vi)	*OSB-to-CFS*	Rigid FO Connector with shear springs	Initial shear stiffness (0.9 kN/mm)	[37]

Note: Given the high OSB-to-CFS connection behaviour variability, associated with the inherent fastener variance and uncertainty of OSB as material [53], the connection behaviour in shear was adopted within limits found in the literature.

4.3. P&P joint behaviour - modelling of the beam-to-column connection

4.3.1. Global behaviour characterization

Before conducting tests on the experimental sub-frames, the utilized P&P joint configurations were tested in accordance with the arrangement depicted in Fig. 25a [48]. Based on the observed experimental response, presented in Fig. 25b by the M-Φ curves, the

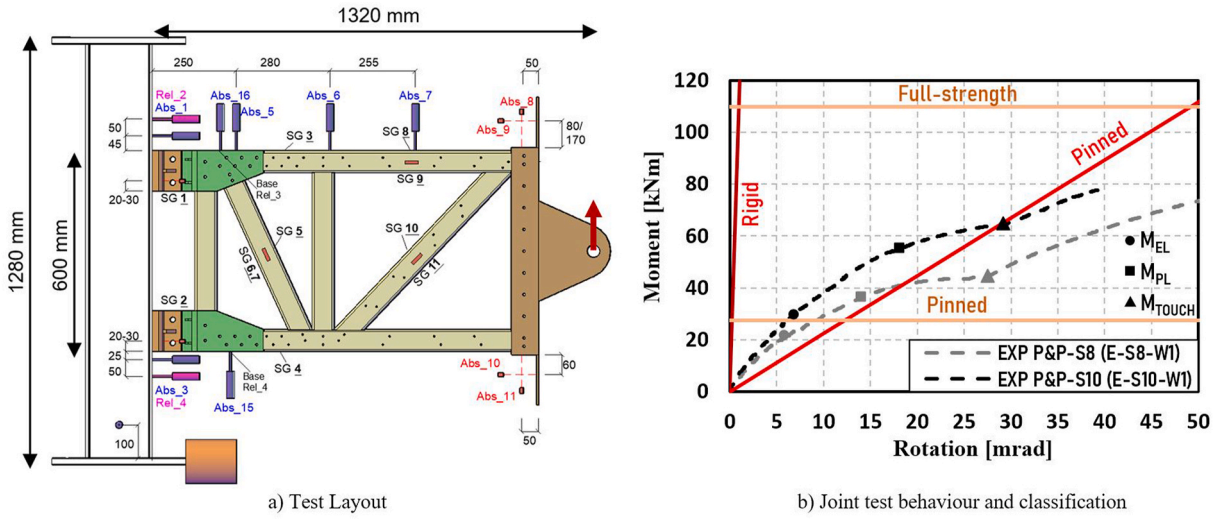

Fig. 25. Experimental M-Φ behaviour of P&P-S8 and P&P-S10 [48] and EN1993-1-8 classification.

P&P-S8 and P&P-S10 can be classified as semi-rigid partial-strength joints, as per EN 1993-1-8 [46] classification. Hence, understanding the joint behaviour in-depth is crucial for accurately predicting the system behaviour.

Therefore, a plan for global characterization of the employed P&P joint configurations was made, with the objective of (i) defining the key joint behaviour governing phenomena and (ii) quantifying their impact, to finally, considering the obtained information, (iii) develop a spring model suitable for global FEM application.

The first step in the global characterization process was to establish a FEM capable of replicating the recorded experimental behaviour of P&P-S8 and P&P-S10. For this purpose, ABAQUS FE software was used.

The model was built upon the work published in Ref. [48], where the conducted experimental campaign on the P&P joint and its components was detailed, base ABAQUS FEM developed and its calibration performed. Analogous modelling strategies were employed herein, together with a few simplifications. The simplifications concerned disregarding the truss and plug-to-truss connection deformability. Indeed, in the initial phase, prior to column-plug contact, the truss had a negligible effect on the recorded M-Φ response of P&P-S8 and P&P-S10. Thus, its deformability was disregarded by modelling the truss as rigid. Similarly, the truss-to-plug connection was modelled as rigid. The parameters such as mesh size, BCs, material properties, interactions, contacts and type of analysis were adopted as in Ref. [48], where additional details can be found.

The FEM comprised several parts: the (i) column, the (ii) socket with bolt-holes, the (iii) M16 bolts, the (iv) plug and the (v) rigid truss (Fig. 26). Nominal dimensions were used, detailed in Ref. [48]. The elastic material properties were defined by MoE of 210 GPa, and Poisson's ratio of 0.3. The plastic material properties were based on true stress – true strain curves, obtained from coupon tests (Fig. 26c). The hardening due to cold-bending was considered. To optimize computational efficiency, symmetry with respect to the longitudinal axis was used, effectively reducing the model to half. The FEM employed C3D8R elements, with the mesh size, number of FE across the thickness and radius division of the curved regions depending on the considered part (Table 10). A minimum of 3 FE across the thickness was used, in order to prevent shear locking. As contact properties, "hard" contact was selected for normal behaviour while employing friction coefficient of 0.2 as a tangential behaviour penalty. Tie constraints were used for modelling the socket-to-column weld connection, as well as for establishing the plug-to-truss connection. The BCs were enforced on both column ends via reference points RP1 and RP2, coupled with the column end faces, restraining all DoF (Fig. 26a). As loading, vertical displacement was introduced at the truss end midpoint, via a node coupled with the truss edge vertical (RP3). Free U1 and R3 were allowed, while all other DoF of RP3 were restrained. Dynamic implicit quasi-static analysis was conducted, in 2 steps. Bolt preload of 62.8 kN was introduced in the initial step, using "bolt load" option, with large deformation/displacement nonlinear effects (Nlgeom) turned off. The loading was applied in the 2nd step, while keeping the bolt length fixed, with Nlgeom option active. Table 10 gives details of the parameters used for each FEM part as well as on the part interactions.

Through a systematically organized parametric study, based on iterative FE analysis and result interpretation, model calibration was performed and FEM validated against EXP results. Beyond the aforementioned, conventionally relevant model attributes, such as mesh size, BCs etc., the response in the elastic stage was found to be strongly influenced by 2 parameters (Fig. 26d): (i) lack of M16 bolt preload (PL) in combination with the presence of bolt-to-hole gap and (ii) T-plug-to-socket clearance, due to installation tolerance (T-plug.tol). The INNO3DJOINTS system does not envision T-plug-to-socket clearance and bolt preload control, as it would compromise the ease-of-assembly concept. Thus, these parameters were not controlled during testing, and were obtained through the calibration process. A very good alignment between experimental and numerical results (Fig. 27, green), for both P&P-S8 and P&P-S10, was achieved by adopting 50 % of the bolt's ultimate tensile strength as preload value, and by considering the initial T-plug-to-socket clearance as 2 mm. Additionally, the influence of these parameters was quantified by extracting the joint response after analysing 2 limit case scenarios: (i) full preload and immediate T-plug-to-socket contact and (ii) no bolt preload and absence of the T-plug (Fig. 27,

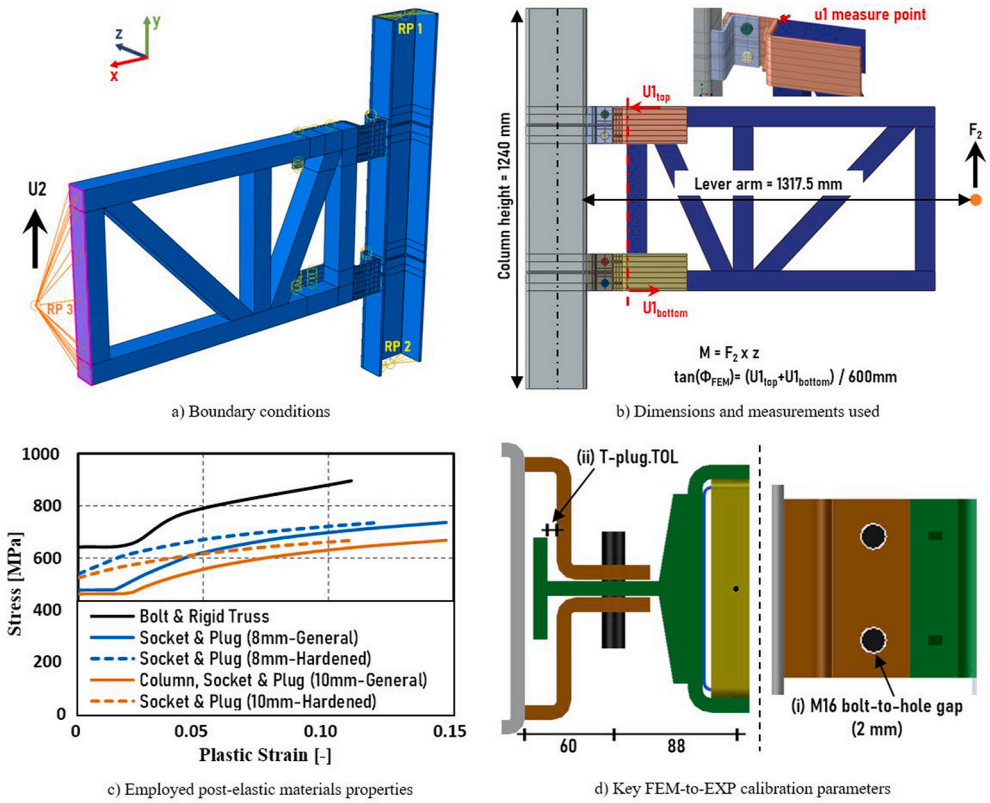

Fig. 26. P&P joint finite element model in ABAQUS. Parts, boundary conditions, employed post-elastic material properties and parameters of key influence for FEM-to-EXP calibration.

red). The discussed parameters were found to have a pronounced effect on the initial elastic stiffness and rotation at the moment of plug-to-column contact.

The analysis of the FEM results allowed to observe an additional phenomena - nearly unobstructed rotation at the socket-to-plug connection region. Already in the initial stage of the loading, relative rotation between the socket and the plug was noted, related to the low level of bolt preload and the presence of bolt-holes. Subsequently, after the hole-gap slip was exceeded, distortional deformation of the socket occurred (Fig. 28). The transversal socket plate distortion was caused by the vertical shear and eccentric axial force, which

Table 10
P&P joint ABAQUS FEM - used parameter details and part interaction.

Name	Column	Socket	Bolts	Plug	Truss
Column	Mesh: 5 mm Radius: 4 divisions 4 FE/thickness	Connection: Tie constraint	–	–	–
Socket		Mesh: 4 mm Radius: 6 divisions 5 FE/thickness	Interaction: surface-surface	Interaction: surface-surface with preload	–
Bolts			Mesh: 2 mm Preload: 62.8 kN	Interaction: surface-surface	–
Plug				Mesh: 5 mm Radius: 6 divisions 3 & 5 FE/thickness	Connection: Tie constraint
Truss					Mesh: 12 mm Fully rigid

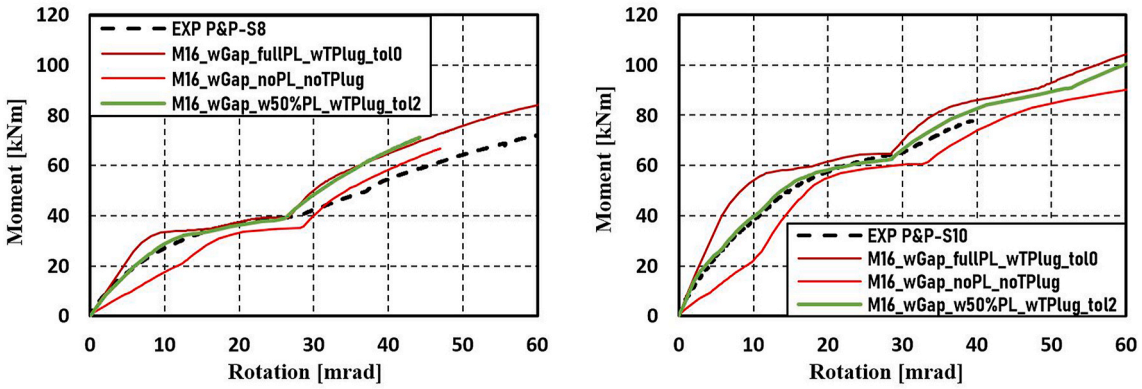

Fig. 27. Experimental versus numerical M-Φ joint behaviour. Impact of the preload and T-plug-to-socket clearance.

induced bending stresses. The observation was confirmed by extracting FEM moment-rotation relationship of significant socket and T-plug cross-sections (Fig. 29). It was concluded that the employed socket configurations, especially the thinner S8, do not provide significant resistance to the distortional deformation, and that the plastic hinge forms in the socket at low values of the bending moment. In addition, at the bolt-hole section nearly no moment development was recorded, while detecting a significant rotation. Thus, it was concluded that the section at the socket-to-plug connection practically behaves as a moment hinge in all loading stages. The phenomena originates from 2 sources (Fig. 28): (i) initial free rotation due to early loss of preload and presence of bolt-to-hole gaps and (ii) distortional socket bending, caused by in-plane bending moment (M_z).

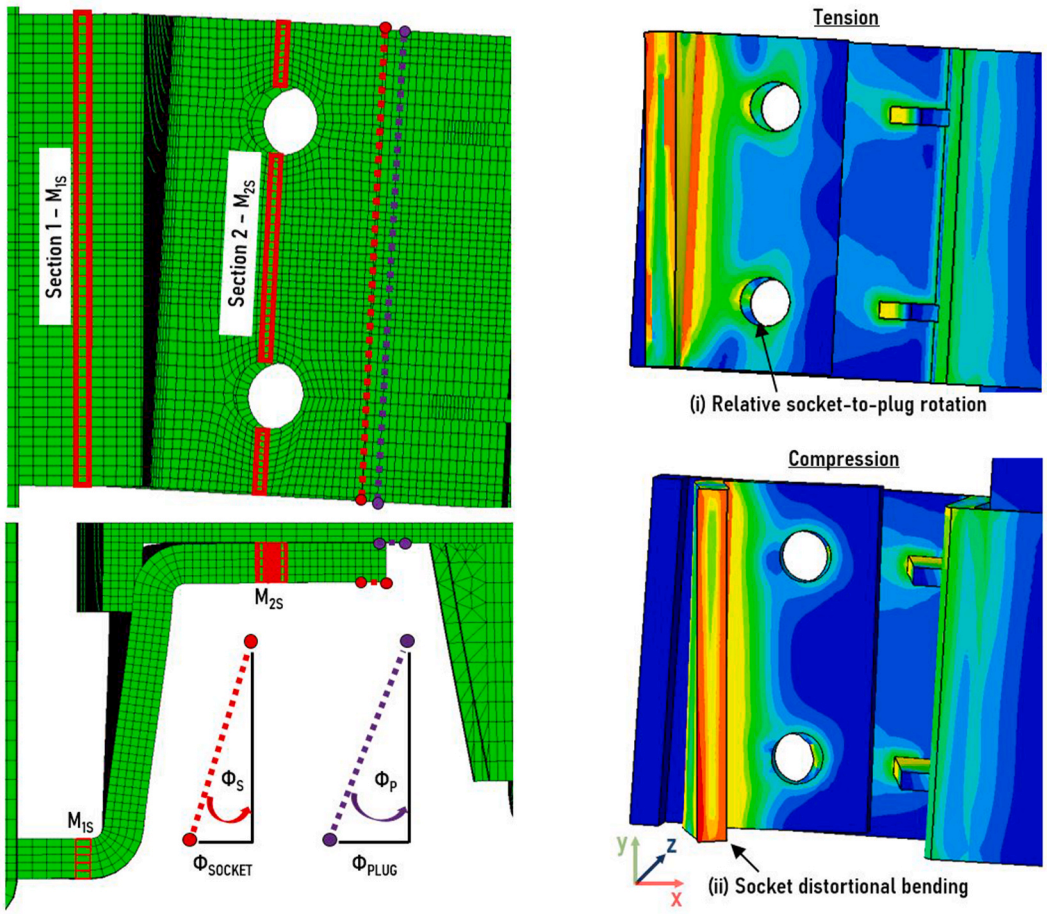

Fig. 28. The observed phenomena and the sections employed for socket-to-plug connection analysis.

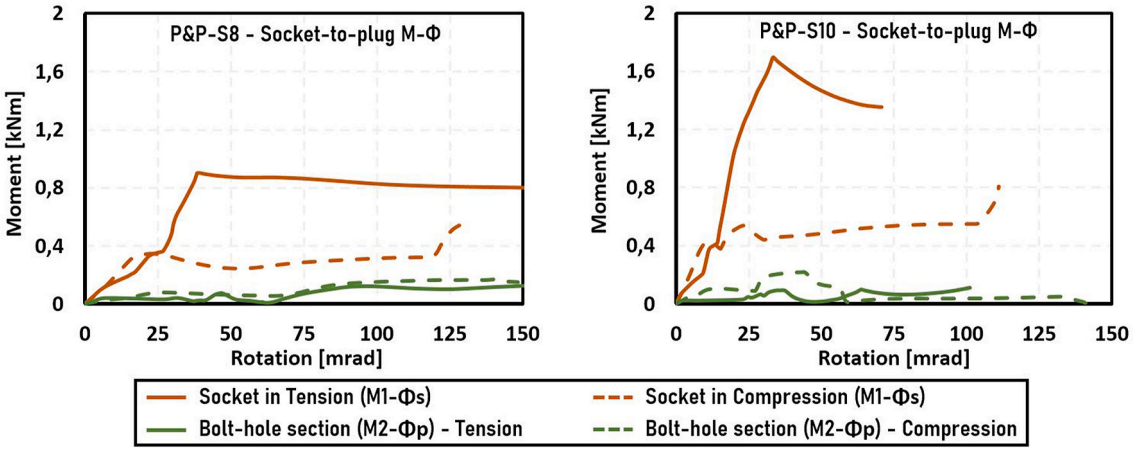

Fig. 29. Socket behaviour in distortional bending and socket-to-plug connection relative rotation.

4.3.2. Spring model for global application

Aiming at modelling the P&P joint effect on the global structure behaviour under monotonic loading, the concept behind the global spring model was to represent each level of the joint by a set of rigid FE, axial and rotational springs, accounting for all significant phenomena.

In application, lacking a validated procedure for obtaining the isolated behaviour of each component, the axial spring behaviour was derived from the experimental M-Φ response, by decomposing the experimental M-Φ curve to a pair of axial springs, considering (i) identical force-displacement behaviour of the 2 springs and (i) fixing the lever arm to the distance between the chord centroids.

The spring model was implement in SAP2000, by employing a rigid FOs, link objects (LO) and end releases (Fig. 30). A rigid FO was used to represent the continuity between the column's centre and its flange. Two-node nonlinear link objects [50] were used to represent the axial springs and apply the derived axial F-δ behaviour, modelling the in-plane M-Φ response. Remaining DoF of the LO

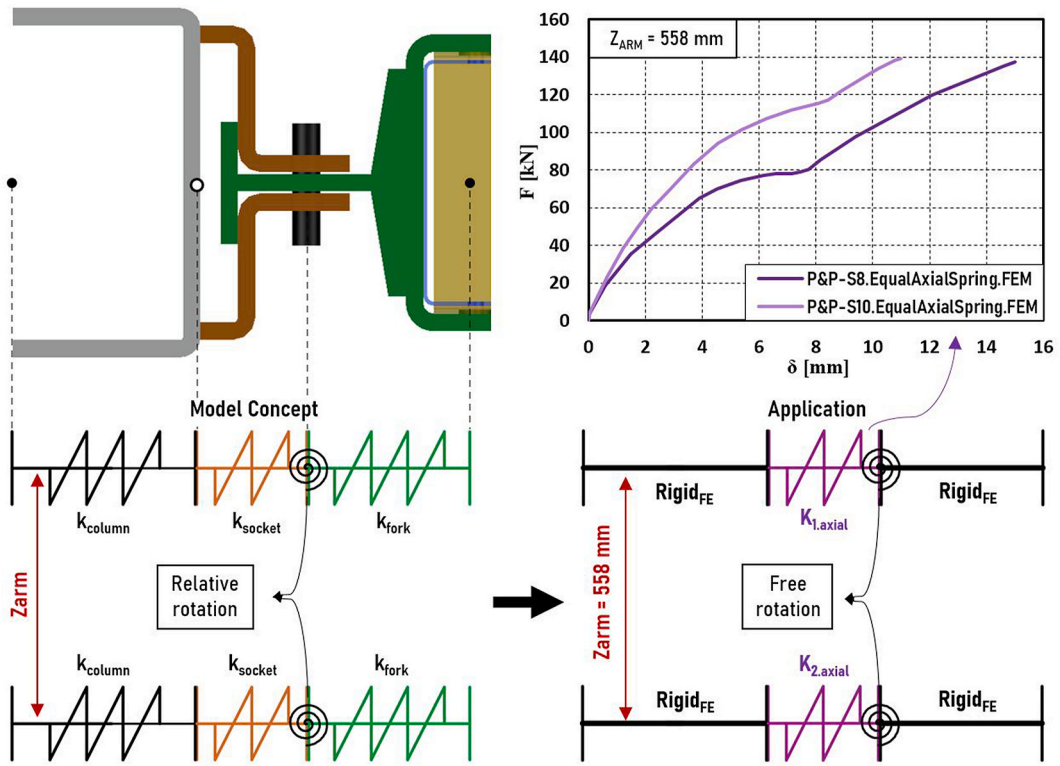

Fig. 30. Global Spring Model. Concept and application. Derived axial spring behaviour applied in SAP2000 based on experimental E-S8-W1 (rep. 2) and E-S10-W1 (rep. 1) behaviour [48] and lever arm Z_{arm} = 558 mm.

were fixed. Another rigid FO was used for representing the continuity between the P&P joint to the truss chord, while accounting for the observed relative rotation phenomena at the position of the socket-to-plug connection by assigning an end moment (M3) release to one of the rigid FO's ends.

4.4. Type of analysis, loading and support conditions

Following the conclusions of the conducted preliminary FEM studies, the influence of imperfections and material nonlinearity were not considered (with the exception of implicit incorporation of these effects by the joint behaviour). Thus, a global static multi-step nonlinear analysis (GNA) was adopted for predicting the structure behaviour. The 2nd-order (P-Δ) effects were accounted for in spite of having a negligible influence on the FEM behaviour, due to the simplicity of their inclusion. The load was applied in increments, as concentrated force assigned in the nodes identified in Fig. 23, acting horizontally or vertically, depending of the modelled specimen. The support conditions of the columns were specified as pinned. The out-of-plane restraint of the top truss chord was not explicitly modelled, instead, a 2D (in-plane) analysis was conducted.

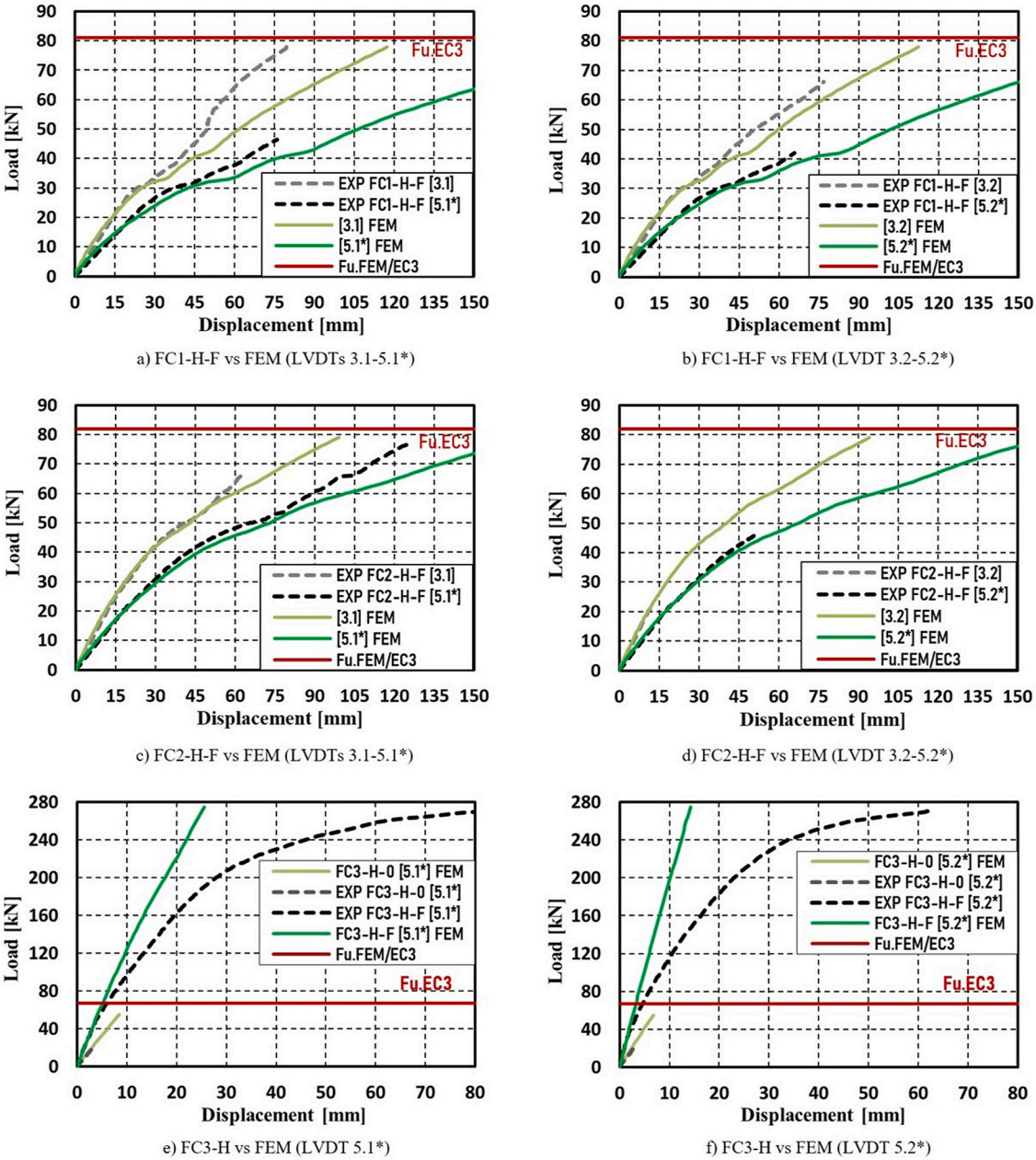

a) FC1-H-F vs FEM (LVDTs 3.1-5.1*)

b) FC1-H-F vs FEM (LVDT 3.2-5.2*)

c) FC2-H-F vs FEM (LVDTs 3.1-5.1*)

d) FC2-H-F vs FEM (LVDT 3.2-5.2*)

e) FC3-H vs FEM (LVDT 5.1*)

f) FC3-H vs FEM (LVDT 5.2*)

Fig. 31. Tests FC1-H-F, FC2-H-F and FC3-H-F vs FEM/EC3 - Horizontal Displacement and Capacity.

4.5. Results and discussion

The comparison between the experimental and numerical results is given in Figs. 31 and 32, while Fig. 33 depicts the FEM obtained deformed shape and shows the location of the estimated failure governing elements. Overall, the proposed model demonstrated satisfying accuracy in predicting the global sub-frame behaviour, in particular the initial stiffness, deformed shape and peak-capacity (FEM internal forces combined with the EC3 design provisions).

In the case of horizontally loaded sub-frame specimens FC1-H and FC2-H (Fig. 31), the modelled behaviour greatly matched the test response in terms of horizontal displacement, for the most part even in the post-elastic phase, confirming the P&P joint as the main source of nonlinearity. Similarly, the FEM response of both FC3-H configurations (with and without OSB) showed good alignment with the test results, however, only in terms of initial stiffness, as the employed modelling strategy limited the model's capability of predicting the post-elastic behaviour of the configurations with the LSF wall (material and OSB-to-CFS connection nonlinearity not considered).

The FEM representing vertically loaded specimens FC1-V and FC2-V was able to accurately predict the experimentally recorded vertical deflection in the elastic stage, which was of main interest (Fig. 32). Again, the post-elastic behaviour, governed by the in-truss deformation, was beyond the model's scope. Nonetheless, the FEM obtained deformed shape was able to portray the experimentally observed shearing of the truss panel segment between the load application points (Fig. 33a). A higher deviation of FEM from EXP results is noted in the case of FC1-V, possibly due to the layout particularities (BC-I and BC-II) affecting the specimen response and the deformed shape. Finally, given the discussed characteristics of the FC3-V experimental response, no attempt of numerically replicating its behaviour was made.

Based on the internal force distribution provided by the developed FEM, the specimen resistance and failure mode was predicted, by applying the EN1993-1-1 and EN1993-1-3 steel member design provisions, and employing experimentally determined material properties.

Overall, the described approach proved fairly applicable. The failure of the specimens FC1-H, FC2-H, FC1-V and FC2-V was predicted in the truss regions affected by the presence of eccentricities (Fig. 33, circled in red), as observed in the experimental campaign, characterized by pronounced influence of shear. The failure was governed either by the combined action of axial compression force and bending (EC3-1-3, Eq. (6.36)), including the additional moments due to the class 4 section centroid shift, or by the interaction of axial tension force, bending moments and shear (EC3-1-3, Eq. (6.27)), as presented in Table 11. Both failure modes had high and closely matched utilization ratios.

In the case of FC1-H and FC2-H, the obtained failure loads slightly overestimated the experimentally recorded values, for 3.7 % and 4.9 %, respectively. However, it should be noted that the peak-capacity was not necessarily reached in these 2 tests, as the load application had to be stopped due to safety concerns at the point of excessive deformation. Moreover, the FEM's inherent limitations, such as employing nominal truss element eccentricities and modelling the P&P joint by assuming both its levels equally stiff, may have resulted in somewhat different internal force distribution compared to the actual experiment, and thus, contributed to the observed discrepancy.

In the case of FC1-V, the estimated failure load closely matched with the load value corresponding to the initially reached plateau in the experimental load-displacement curve, observed at around 130 kN (Fig. 32a). However, the failure was delayed and the specimen was able to sustain additional load, due to the deformability allowed by the employed BC, as previously described. As it regards the specimen FC2-V, the estimated failure load greatly matched the experimentally recorded capacity, differing only by 2.4 %, on the safe side.

Due to its robust nature, the specimen FC3-H was capable of sustaining additional load after the initial member had failed. However, the employed approach was able only to predict the failure of the first element (Fig. 33). The failure was estimated to be governed by the combined action of axial compression force and bending (EC3-1-3, Eq. (6.36)), localized at the corner of the LSF wall

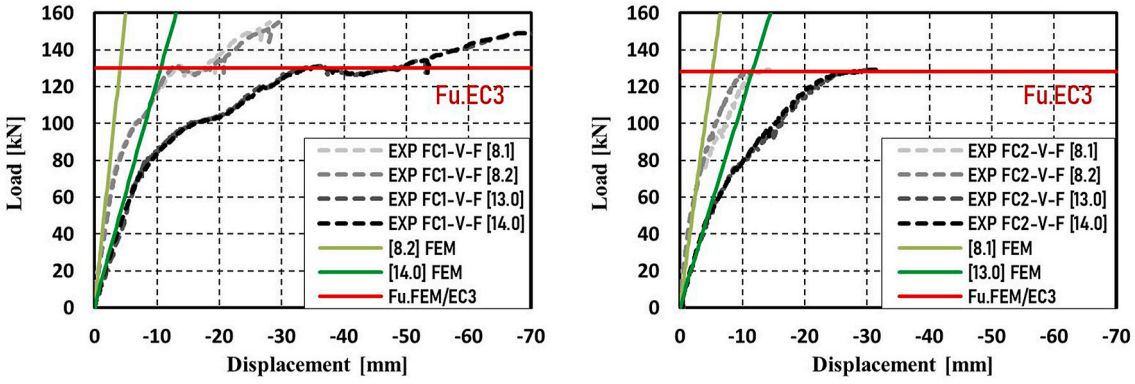

a) FC1-V-F vs FEM (LVDTs 8.1-8.2-13.0-14.0)

b) FC2-V-F vs FEM (LVDTs 8.1-8.2-13.0-14.0)

Fig. 32. Tests FC1-V-F and FC2-V-F vs FEM/EC3 - Vertical Deflection and Capacity.

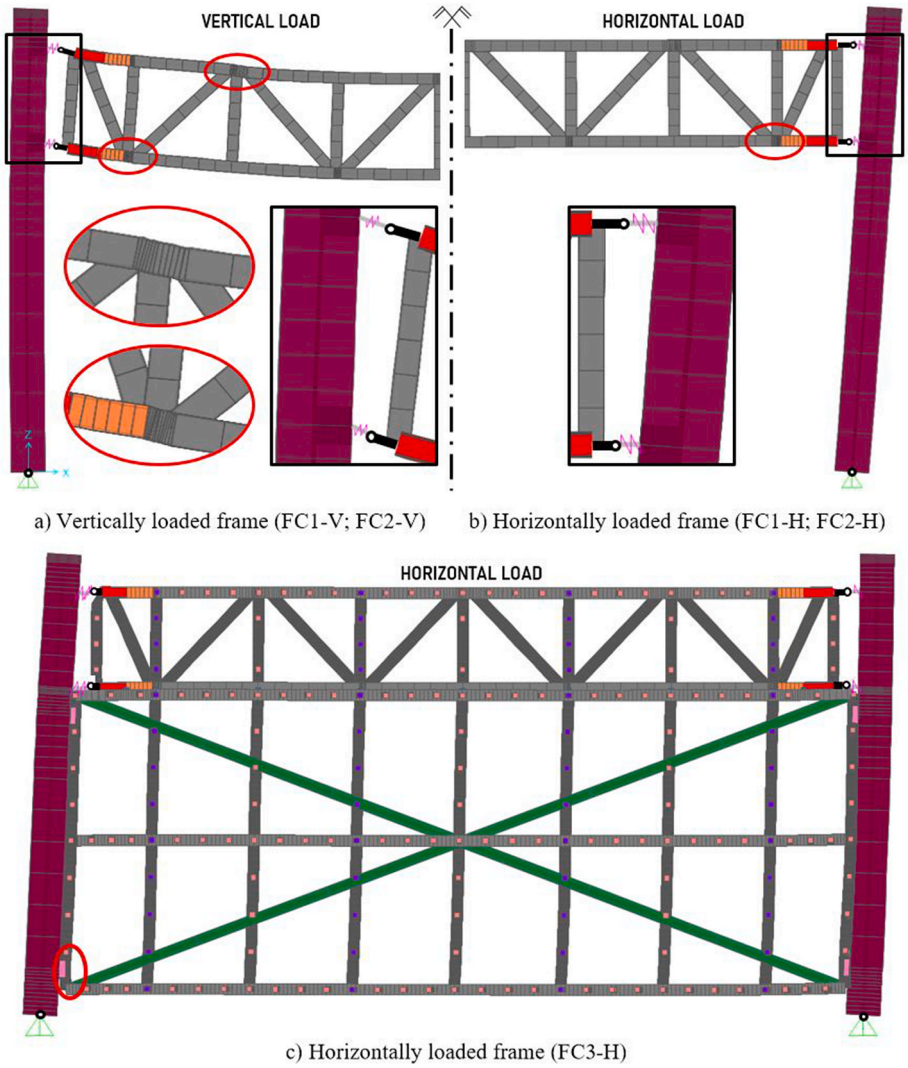

Fig. 33. Deformed shape and location of the FEM/EC3 failure governing elements.

edge stud. Indeed, the eccentricity of the column-to-wall connection lead to high bending moments in the edge stud corner region. Excessive deformation in the same zone was also noted in the experimental campaign.

Moreover, the system performance was compared with the estimated Eurocode serviceability limit state (SLS) demand in terms of horizontal ($k_{hor.EC.SLS}$) and vertical stiffness ($k_{vert.EC.SLS}$). For this purpose, the open frame solution specimens were considered as frames of a category A residential building, located in Coimbra, Portugal, subjected to self-weight and utilization load as vertical actions, and wind as the only horizontal action (effective width of 5 m assumed). The recorded truss-girder vertical stiffness proved adequate, satisfying the demand by a high margin ($k_{vert.EC.SLS} = 5.10$ kN/mm). On the other hand, the measured horizontal stiffness of the tested single-span frame configurations failed to meet Eurocode requirements ($k_{hor.EC.SLS} = 3.63$ kN/mm). However, the numerical analysis results indicate that changing the column support conditions to fixed, in combination with P&P-S10, could satisfy the $k_{hor.\ SLS.\ req}$ demand. Moreover, employing multi-span frame configurations, which reflects better the more common application scenario, could result in fulfilling the necessary conditions for system's use without bracing or fixed column support.

Table 11
Load-bearing capacity - EXP vs NUM/EC3.

Specimen	FC1-H	FC2-H	FC3-H	FC1-V	FC2-V
Load-bearing capacity - EXP [kN]	79	77	269	155	129
Load-bearing capacity - NUM/EC3 [kN]	82	81	68	130	126
Governing equation - NUM/EC3	Eq. 6.36/6.27	Eq. 6.36	Eq. 6.36	Eq. 6.36/6.27	Eq. 6.27/6.36

Note: Peak-capacity was not reached in every test, as the load application had to be stopped due to safety concerns at the point of excessive deformation.

5. Conclusions

An experimental investigation was conducted on the INNO3DJOINTS novel hybrid modular construction system, comprising (i) EN 10219 based steel tubular columns, and (ii) CFS thin-wall section based truss-girders, joint together by the (iii) innovative bolt-based P&P connector. A total of 6 full-scale sub-frame specimens were subjected to 2 loading scenarios: (i) horizontal and (ii) vertical loading. The specimens differed in the utilized P&P joint configuration and the presence/absence of the light-steel framing wall, encased with OSB, resulting in 3 distinct sub-frame configurations (2 open and 1 closed frame solution).

The conducted experimental campaign lead to the following conclusions:

(1) The INNO3DJOINTS open sub-frame solutions demonstrated high deformability and load-bearing capacity. The specimen failure was governed by the stress concentration in the truss node regions, aggravated by the presence of eccentricities. Local buckling, most often accompanied with the net-section tearing, was identified as the predominant failure mode, highlighting the need for improved control of the in-truss screw spacing, as well as minimization of eccentricity occurrence and impact. Next to the more centric element positioning, future research could explore employing thicker CFS profiles, especially for the truss chords, as well as using alternative screw disposition for in-truss connections. Under horizontal loading, the employed P&P joint configuration had significant impact on the specimen response, being the main source of deformability and affecting the initial elastic horizontal stiffness by up to 25 %. The recorded horizontal stiffness proved insufficient to satisfy the estimated Eurocode SLS demand (assumed action wind, location Coimbra, Portugal), however, for pinned column support conditions, semi-rigid joint configurations and a single-span frame. Future research should include investigating multi-span frame configurations, defining the system's scope of use and its potential for functioning without an external, on-site constructed bracing system, and/or fixed column supports. Under vertical loading, the joint selection appeared to have negligible effect on the specimen response. The specimens exhibited nearly identical vertical deflection in the elastic stage, with the main source of deformability located in the truss panel nodes. For the considered span of nearly 5 m, the system demonstrated satisfying vertical stiffness compared to the SLS demand (category A residential building self-weight and utilization loads considered), while showing no necessity for bracing the truss bottom chord out-of-plane displacement, even at the ultimate load, adding to the system's architectural flexibility.

(2) The LSF wall addition greatly contributed to the sub-frame stiffness and ultimate capacity. An increase of roughly 350 % and 640 % in ultimate capacity was recorded under horizontal and vertical loading, respectively. In terms of initial horizontal stiffness, equipping a sub-frame with a bare LSF wall (no OSB) resulted in an increase of around 550–600 %, while the additional OSB application (2×12.5 mm OSB/2) enhanced the bare LSF wall contribution by 200–280 %. The LSF wall presence also affected the failure mode. Under vertical load, the collapse was governed by the combined effect of flexural and local-distortional buckling of the truss vertical. Under horizontal load, the closed sub-frame solution exhibited a progressive collapse. A successive failure of bolts in shear of the column-to-wall stud connection was observed during the test, while the post-test OSB panel removal revealed deformation of the wall stud in the connection vicinity, as well as the local buckling of the compressed truss top chord. The observed behaviour underlined the importance of providing a stronger column-to-wall connection, while minimizing its eccentricity. The potential of employing the P&P joint for the column-to-wall connection could be explored in the future, as it could facilitate the wall installation and standardize the production. The OSB remained intact until reaching near ultimate capacity, suggesting that the number of screws of the OSB-to-CFS connection could be optimized.

(3) The P&P joint utilization proved successful in facilitating the assembly process, one of the key system features. The employed joint configuration had a significant impact on the response of the wall-free specimens loaded horizontally, while it appeared to have no effect on the vertical stiffness, ultimate capacity and failure mode of the specimens. Both P&P-S8 and P&P-S10 exhibited ductile behaviour, with the deformation mostly localized in the socket. Given the envisioned dissipative role of the socket, future studies could address the feasibility and the trade-offs associated with a detachable column-to-socket connection.

Based on the sub-frame experimental results and conclusions, as well as the isolated joint tests [48], a FEM model was developed, comprising 2 phases: (i) P&P joint characterization leading to a spring model and (ii) implementation of the joint model into the global frame model.

In the 1st stage, the P&P joint FEM calibration and validation was performed, key behaviour governing phenomena defined, leading to a spring model for global application. The following was concluded:

(1) Next to the traditional parameters (geometry, material, etc.), 2 factors significantly impact the P&P joint behaviour: (i) bolt preload together with the bolt-to-hole gap and (ii) T-plug-to-socket clearance. With the ease-of-assembly as the system's priority, the on-site control of these parameters is not envisioned, however, their influence should be factored in the future research and design. The option of removing the T-plug or ensuring it does not interact with other connection elements by reducing its size could be explored.

(2) Nearly unobstructed rotation in the socket-to-plug connection region, throughout all loading stages, was noted. The phenomenon was attributed to 2 factors: (i) initial free rotation due to early preload loss and bolt-to-hole gaps, and (ii) subsequent distortional socket bending induced by in-plane moments. Postponing the observed rotation, together with increasing the socket's stiffness and elastic resistance limit, possibly by employing socket configurations with stiffeners and/or increasing plate thickness, could benefit the system's global behaviour.

In the 2nd stage, the spring model was implemented into the global FEM developed in SAP2000. The FEM was based on 1D beam FEs (only OSB represented by shell FEs), while introducing inter-element connectivity through releases and discrete connectors. It was concluded that:

(1) The proposed FEM is capable of accurately replicating the global behaviour of all modelled test specimens in the elastic range, namely the initial stiffness and the deformed shape.
(2) In the case of open frame specimens loaded horizontally, the FEM response was closely aligned with the test results even in the post-elastic stage, affirming the P&P joint as the main source of nonlinearity and validating the proposed joint spring model.
(3) In the case of closed frame solution modelling, FC3-H, the eccentricity of column-to-wall connection proved to significantly influence the response under horizontal load. Likewise, the influence of OSB-to-CFS connection stiffness was found relevant.
(4) Based on the FEM internal force distribution, by employing EN1993-1-1 and EN1993-1-3 steel member design provisions and experimental material properties, it was possible to predict the failure load of the wall-free specimens. The failure was predicted in the truss node regions, affected by eccentricities, as observed in the experimental campaign, characterized by pronounced influence of shear. The estimated ultimate capacity closely matched the experimental one, with a discrepancy of less than 5 %, except in the case of FC1-V.

Finally, it is worth mentioning that the INNO3DJOINTS system has been further investigated by performing tests on a full-scale building, transitioning from a 2D to a 3D study, which will be reported in the following publications.

CRediT authorship contribution statement

Nemanja Milovanović: Formal analysis, Investigation, Methodology, Validation, Visualization, Writing – original draft, Writing – review & editing. **Trayana Tankova:** Investigation, Methodology, Supervision, Validation, Writing – review & editing. **Rui Simões:** Investigation, Methodology, Supervision, Writing – review & editing. **Luís Carlos Silva:** Formal analysis. **Hélder David Craveiro:** Formal analysis, Investigation, Writing – review & editing. **Ricardo Costa:** Investigation, Writing – review & editing. **Cláudio Martins:** Investigation. **Luís Simões da Silva:** Conceptualization, Supervision, Writing – review & editing.

Declaration of competing interest

The authors declare that they have no known competing financial interests or personal relationships that could have appeared to influence the work reported in this paper.

Data availability

Data available upon personal request and with a valid explanation.

Acknowledgements

The work and results presented herein were made possible through funding from the following sources: (i) FCT / MCTES through national funds (PIDDAC) under the R&D Unit Institute for Sustainability and Innovation in Structural Engineering (ISISE), under reference UIDB / 04029/2020; (ii) National funds through FCT - Foundation for Science and Technology, under grant agreement 2020.08384.BD attributed to the 1st author; (iii) European Community's Research Fund for Coal and Steel (RFCS), project INNO3DJOINTS No.749959; (iv) Portuguese Ministry of Science, Technology and Higher Education (Ministério da Ciência, Tecnologia e Ensino Superior) under the project contract Grant INNO3DJOINTS (031834). The authors would like to credit the laboratory personnel, namely Miguel Queiroz and João Vidal, for their contribution to the experimental campaign realization.

References

[1] R.M. Lawson, P.J. Grubb, J. Prewer, P.J. Trebilcock, Modular Construction Using Light Steel Framing: an Architect's Guide, 1 ed., Steel Construction Institute, 1999, p. 105. P272.
[2] M. Tenório, R. Ferreira, V. Belafonte, F. Sousa, C. Meireis, M. Fontes, I. Vale, A. Gomes, R. Alves, S.M. Silva, D. Leitão, A.C. Fontes, C. Maia, A. Camões, J. M. Branco, Contemporary strategies for the structural design of multi-story modular timber buildings: a comprehensive review, Appl. Sci. (2024), https://doi.org/10.3390/APP14083194.
[3] R.M. Lawson, R.G. Ogden, Hybrid' light steel panel and modular systems, Thin-Walled Struct. 46 (7) (2008) 720–730, https://doi.org/10.1016/j.tws.2008.01.042.
[4] R. M. Lawson, "Light Steel Modular Construction," Steel Construction Institute, Technical Information Sheet ED010-ED014. Accessed: 22.06.2022. [Online]. Available: https://steel-sci.com/assets/downloads/LSF/ED01420Download.pdf.
[5] H.-T. Thai, T. Ngo, B. Uy, A review on modular construction for high-rise buildings, Structures 28 (2020) 1265–1290, https://doi.org/10.1016/j.istruc.2020.09.070.
[6] M. Lawson, R. Ogden, C.I. Goodier, Design in Modular Construction, 1 ed., CRC Press, Boca Raton, FL, 2014, p. 280.
[7] M. Mortazavi, P. Sharafi, H. Ronagh, B. Samali, K. Kildashti, Lateral behaviour of hybrid cold-formed and hot-rolled steel wall systems: experimental investigation, J. Constr. Steel Res. 147 (2018) 422–432, https://doi.org/10.1016/j.jcsr.2018.04.035.
[8] P. Gatheeshgar, K. Poologanathan, S. Gunalan, K.D. Tsavdaridis, B. Nagaratnam, E. Iacovidou, Optimised cold-formed steel beams in modular building applications, J. Build. Eng. 32 (2020) 101607, https://doi.org/10.1016/j.jobe.2020.101607.
[9] S. Navaratnam, D. Widdowfield Small, P. Gatheeshgar, K. Poologanathan, J. Thamboo, C. Higgins, P. Mendis, Development of cross laminated timber-cold-formed steel composite beam for floor system to sustainable modular building construction, Structures 32 (2021) 681–690, https://doi.org/10.1016/j.istruc.2021.03.051.

[10] F.E. Boafo, J.-H. Kim, J.-T. Kim, Performance of modular prefabricated architecture: case study-based review and future pathways, Sustainability 8 (6) (2016) 558, https://doi.org/10.3390/su8060558.
[11] I.J. Ramaji, A.M. Memari, Identification of structural issues in design and construction of multi-story modular buildings, in: Proceedings of the 1st Residential Building Design and Construction Conference, 2013, pp. 294–303.
[12] T. Salama, A. Salah, O. Moselhi, M. Al-Hussein, Near optimum selection of module configuration for efficient modular construction, Autom. ConStruct. 83 (2017) 316–329, https://doi.org/10.1016/j.autcon.2017.03.008.
[13] W. Pan, Y. Yang, L. Yang, High-rise modular building: ten-year journey and future development, in: Construction Research Congress, New Orleans, 2018, pp. 523–532.
[14] S. Srisangeerthanan, M.J. Hashemi, P. Rajeev, E. Gad, S. Fernando, Review of performance requirements for inter-module connections in multi-story modular buildings, J. Build. Eng. 28 (2020) 101087, https://doi.org/10.1016/j.jobe.2019.101087.
[15] D.-A. Corfar, K.D. Tsavdaridis, A comprehensive review and classification of inter-module connections for hot-rolled steel modular building systems, J. Build. Eng. 50 (2022) 104006, https://doi.org/10.1016/j.jobe.2022.104006.
[16] X. Liu, A. Zhang, J. Ma, Y. Tan, Y. Bai, Design and model test of a modularized prefabricated steel frame structure with inclined braces, Adv. Mater. Sci. Eng. 2015 (2015), https://doi.org/10.1155/2015/291481.
[17] K. Khan, Z. Chen, J. Liu, K. Javed, State-of-the-Art on technological developments and adaptability of prefabricated industrial steel buildings, Appl. Sci. (2023), https://doi.org/10.3390/APP13020685.
[18] A.W. Lacey, W. Chen, H. Hao, "Experimental Methods for Inter-module Joints in Modular Building Structures – A State-Of-The-Art Review,", 2021, https://doi.org/10.1016/J.JOBE.2021.103792.
[19] J. Liew, Y. Chua, and Z. Dai, "Steel concrete composite systems for modular construction of high-rise buildings," in Structures, 2019, vol. 21: Elsevier, pp. 135–149, doi:https://doi.org/10.1016/j.istruc.2019.02.010.
[20] W. Ferdous, Y. Bai, T.D. Ngo, A. Manalo, P. Mendis, New advancements, challenges and opportunities of multi-storey modular buildings–A state-of-the-art review, Eng. Struct. 183 (2019) 883–893, https://doi.org/10.1016/j.engstruct.2019.01.061.
[21] C. Loss, B. Davison, Innovative composite steel-timber floors with prefabricated modular components, Eng. Struct. 132 (2017) 695–713, https://doi.org/10.1016/j.engstruct.2016.11.062.
[22] S. Pastori, E.S. Mazzucchelli, M. Wallhagen, "Hybrid Timber-Based Structures: A State of the Art Review,", 2022, https://doi.org/10.1016/J.CONBUILDMAT.2022.129505.
[23] CHRISTMANN+PFEIFER, C+P modular [Online]. Available: https://www.cpbau.de/en/products/c-p-modular-building.
[24] THINKWOOD, Brock commons tallwood house [Online]. Available: https://www.thinkwood.com/projects/brock-commons-tallwood-house.
[25] MODSCAPE, CLT: making modular even more sustainable [Online]. Available: https://www.modscape.com.au/blog/clt-modular-more-sustainable/.
[26] SKENDER, Skender modular construction [Online]. Available: https://www.skender.com/.
[27] O. Pons, Assessing the sustainability of prefabricated buildings, in: Eco-efficient Construction and Building Materials, Elsevier, 2014, pp. 434–456.
[28] C. Loss, M. Piazza, R. Zandonini, Connections for steel–timber hybrid prefabricated buildings. Part II: innovative modular structures, Construct. Build. Mater. 122 (2016) 796–808, https://doi.org/10.1016/j.conbuildmat.2015.12.001.
[29] F. Ascione, F. Esposito, G. Iovane, D. Faiella, B. Faggiano, E. Mele, Sustainable and efficient structural systems for tall buildings: exploring timber and steel–timber hybrids through a case study, Buildings (2024), https://doi.org/10.3390/BUILDINGS14020524.
[30] I. Becker, F. Anderson, A.R. Phillips, Structural design of hybrid steel-timber buildings for lower production stage embodied carbon emissions, J. Build. Eng. (2023), https://doi.org/10.1016/J.JOBE.2023.107053.
[31] C. Loss, M. Piazza, R. Zandonini, Connections for steel–timber hybrid prefabricated buildings. Part I: experimental tests, Construct. Build. Mater. 122 (2016) 781–795, https://doi.org/10.1016/j.conbuildmat.2015.12.002.
[32] P. Santos, L. Simões da Silva, V. Ungureanu, Energy Efficiency of Light-Weight Steel-Framed Buildings; European Convention for Constructional Steelwork (ECCS), Google Scholar, Brussels, Belgium, 2012.
[33] MAXISPAN, Maxispan steel building frames [Online]. Available: https://maxispan.com.au/.
[34] COGI, steelMAX - modular construction system [Online]. Available: http://www.steelmax.it/en/.
[35] R. Landolfo, Lightweight steel framed systems in seismic areas: current achievements and future challenges, Thin-Walled Struct. 140 (2019) 114–131, https://doi.org/10.1016/j.tws.2019.03.039.
[36] R. Landolfo, L. Fiorino, G.D. Corte, Seismic behavior of sheathed cold-formed structures: physical tests, J. Struct. Eng. 132 (4) (2006) 570–581, https://doi.org/10.1061/(ASCE)0733-9445(2006)132:4(570).
[37] J. Henriques, N. Rosa, H. Gervasio, P. Santos, L.S. da Silva, Structural performance of light steel framing panels using screw connections subjected to lateral loading, Thin-Walled Struct. 121 (2017) 67–88, https://doi.org/10.1016/j.tws.2017.09.024.
[38] M.J. Rukavina, D. Skejić, A. Kralj, T. Ščapec, B. Milovanović, "Development of lightweight steel framed construction systems for nearly-zero, Energy Build. (2022), https://doi.org/10.3390/BUILDINGS12070929.
[39] M.J. Rukavina, D. Skejić, B. Milovanović, T. Ščapec, Fire tests of load-bearing, light-steel-framed wall systems insulated with polyurethane foam, Appl. Sci. (2024), https://doi.org/10.3390/APP14020637.
[40] M. Zeynalian, H.R. Ronagh, S. Hatami, Seismic characteristics of K-braced cold-formed steel shear walls, J. Constr. Steel Res. 77 (2012) 23–31, https://doi.org/10.1016/j.jcsr.2012.04.009.
[41] M. Mortazavi, P. Sharafi, K. Kildashti, B. Samali, Prefabricated hybrid steel wall panels for mid-rise construction in seismic regions, J. Build. Eng. (2020), https://doi.org/10.1016/J.JOBE.2019.100942.
[42] N. Usefi, P. Sharafi, M. Mortazavi, H.R. Ronagh, B. Samali, Structural performance and sustainability assessment of hybrid-cold formed modular steel frame, J. Build. Eng. (2021), https://doi.org/10.1016/J.JOBE.2020.101895.
[43] PRESCIENT, Prescient Co inc | revolitionize the building environment [Online]. Available: https://prescientco.com/.
[44] R. Simões, S. Jordão, J. Diogo, J. Fernandes, Development and design of a concealed splice joint configuration between tubular sections, Eng. Struct. 137 (2017) 181–193, https://doi.org/10.1016/j.engstruct.2017.01.054.
[45] CEN, Eurocode 3 - Design of Steel Structures - Part 1-3: General Rules - Supplementary Rules for Cold-Formed Members and Sheeting, European Committee for Standardization, Brussels, 2006.
[46] CEN, Eurocode 3 - Design of Steel Structures - Part 1-8: Design of Joints, European Committee for Standardization, Brussels, 2005.
[47] INNO3DJOINTS, "Innovative 3D joints for robust and economic hybrid tubular construction," RFCS - Agreement No: 749959, final report.
[48] T. Tankova, H. Craveiro, L.C. Silva, F.F. Ribeiro, R. Simões, C. Martins, R. Costa, L. Simões da Silva, Behaviour of plug-and-play joints between RHS columns and CFS trusses, Structures 41 (2022) 1719–1745, https://doi.org/10.1016/j.istruc.2022.05.099.
[49] L. Simões da Silva, L.C. Silva, T. Tankova, H.D. Craveiro, R. Simões, R. Costa, M. D'Aniello, R. Landolfo, Performance of modular hybrid cold-formed/tubular structural system, Structures 30 (2021) 1006–1019, https://doi.org/10.1016/j.istruc.2021.01.066.
[50] CSI, "Cold Formed Steel Frame Design Manual EC 3-1-3 2006 for SAP2000,", 2021.
[51] J. Porteous, A. Kermani, Structural Timber Design to Eurocode 5, John Wiley & Sons, 2013.
[52] M.S. Lemma, C. Rebelo, L.S. da Silva, Eurocode 8 revision–Implications on the design and performance of steel moment-resisting frames: case study, Soil Dynam. Earthq. Eng. 161 (2022) 107411, https://doi.org/10.1016/j.soildyn.2022.107411.
[53] F. Derveni, S. Gerasimidis, B.W. Schafer, K.D. Peterman, High-fidelity finite element modeling of wood-sheathed cold-formed steel shear walls, J. Struct. Eng. 147 (2) (2021) 04020316, https://doi.org/10.1061/(ASCE)ST.1943-541X.0002879.

[54] C.V. Miculaş, R. Costa, L.S. da Silva, R. Simões, H.D. Craveiro, T. Tankova, 3D macro-element for innovative plug-and-play joints, J. Constr. Steel Res. (2024), https://doi.org/10.1016/J.JCSR.2023.108436.
[55] H.D. Craveiro, R. Rahnavard, L. Laím, R.A. Simões, A. Santiago, Buckling behavior of closed built-up cold-formed steel columns under compression, Thin-Walled Struct. 179 (2022) 109493, https://doi.org/10.1016/j.tws.2022.109493.
[56] A. Ahmed, L.H. Teh, Thread effects on the stiffness of bolted shear connections, J. Constr. Steel Res. 160 (2019) 77–88, https://doi.org/10.1016/j.jcsr.2019.05.023.